Page left blank

Preface and Acknowledgments

The writing of this thesis, and the experimental work presented within, has been conducted in the Chemosensory lab at the Department of Psychology (Norwegian University of Science and Technology; NTNU). This experience has granted me insight into a field and methodologies which I knew little of beforehand. For this, I first and foremost thank my main supervisor, Xi Chu, who has granted me more of her time, knowledge, and guidance than any student could expect from their supervisor. Additionally, she gathered half of the data used in the statistical analyses. Also, Gerit Pfuhl, my co-supervisor, has been a reliable source of benevolence. If she had not taught me on the use of electrophysiological data, such analyses could not have been performed. In fact, without the ideas of Xi and Gerit, I would not have had an opportunity to put my appreciation for statistical analyses to use, and this thesis would have taken a very different form.

I would also like to thank my second co-supervisor, and leader of the chemosensory lab, Bente Gunnveig Berg. Without Bente there would be no opportunity for psychology students to work directly with the central nervous system. Her familiarity with the model organism, and willingness to offer insights on everything from methodology to anatomy, has been most appreciated. In addition, Hanna Mustaparta, Elena Ian, Pramod KC, Ida Camilla Kjos and Andreas Panayiotis Goustas have all offered their insights and help on many occasions. The researcher Mikhail Zhemchuzhnikov, who worked in the lab during my first three months there, proved knowledgeable and inspirational in my first and most challenging months at the lab. I owe you all my thanks. As for my fellow master students at the lab, Mari Reitstøen Arnesen, Rose Hodson and Maja Juell, I thank you all for good discussions, your insights and your comradery.

At last, I would like to offer my sincerest gratitude to my wife, Eneda Kymre, for supporting my pursuit of academic achievements, and for taking such good care of our two children, Alva and Edvard, while I have been immersed in my studies. Thank you very much! Also, I must thank my dear daughter Alva, who reminded me that the “white butterflies” were to be treated kindly.

Jonas Hansen Kymre

Abstract

Individual neurons can be characterized by their electrophysiological activity. Such characterizations have helped researchers investigate the functioning of individual neurons and neural networks consisting of distinct neuron categories. In the primary olfactory center of the insect brain, the antennal lobe, electrophysiological characterizations have in large part focused on the alterations in activity during odor stimulation. In comparison, the background on which neural responses occur, i.e. the spontaneous activity, has been sparsely described. Attempts to identify neuron categories in the antennal lobe, using physiological parameters of spontaneous spiking activity, has only been performed in one study. It demonstrated that physiology can indeed be used to predict morphology.

In this thesis, *in vivo* intracellular recording and staining, combined with confocal microscopy, was performed in the noctuid moth *Helicoverpa armigera* to gather physiological and neuroanatomical data on two types of antennal lobe neurons; local interneurons and projection neurons. The main purpose of the study is to investigate whether these two morphologically different neuron categories can be identified by their spontaneous spiking patterns. The results approved that the spontaneous activity could be used as an indicator to identify neuron category without morphological classification, and the correct classification rate is up to 76%. In addition, we investigated whether sub-categories of projection neurons could be identified. However, identified clusters had no significant association with morphological features, neither dendritic arborizations, nor confinement to antennal lobe tract.

Moreover, this thesis includes novel findings on projection neuron morphology. As many as three neurons confined to the recently discovered transverse antennal lobe tract were identified here.

Abbreviations

ACC	Anterior cell body cluster
AL	Antennal lobe
ALT	Antennal lobe tract
AVLP	Anterior ventro-lateral protocerebrum
cV	Coefficient of variation
FF	Fano factor
FWHM	Full-width at half maximum
GABA	γ-aminobutyric acid
INP	Inferior neuropil
ISI	Interspike interval
lALT	Lateral antennal lobe tract
LCC	Lateral cell body cluster
LH	Lateral horn
LN	Local interneuron
LPOG	Labial-palp pit organ glomerulus
mALT	Medial antennal lobe tract
MB	Mushroom bodies
MCC	Medial cell body cluster
MGC	Macroglomerular complex
mlALT	Medio-lateral antennal lobe tract
OG	Ordinary glomeruli
OSN	Olfactory sensory neuron
PCx	Posterior complex
PLP	Postero-lateral neuropil
PN	Projection neuron
PSTH	Peri-stimulus histogram
SNP	Superior neuropil
tALT	Transverse antennal lobe tract
VMNP	Ventro-medial neuropil

Table of content

Page left blank

1. Introduction

In the nervous system, information is often encoded as series of action potentials (spike trains). Within a neuron, this appears as distinct and largely homogeneous spikes of electrical activity. By summation of temporally coherent inputs from presynaptic neurons, a postsynaptic action potential can be initiated if the sum of excitatory and inhibitory synapses brings the intracellular voltage to the action potential threshold (reviewed by Siegelbaum, Kandel, & Yuste, 2013). When this occurs, change in membrane permeability to sodium (Na^+) causes extracellular Na^+ to enter the neuron. The inward Na^+ current causes a depolarization, which is an increase in the intracellular voltage relative to the extracellular voltage, this may lead to neurotransmitter-release from the presynaptic terminals. After reaching equilibrium potential for Na^+, i.e. when Na^+ does not flow in or out of the neuron, an outward current of potassium (K^+) leads to hyperpolarization. This is a decrease in the transmembrane potential which leads to the neuron`s charge getting even lower than resting potential (Hodgkin & Huxley, 1952; reviewed by Koester & Siegelbaum, 2013a).

For any postsynaptic neuron, there is a summation of various inputs from a potentially vast number of presynaptic terminals. The interconnectedness of numerous neurons, and the presence of inhibitory and excitatory neurotransmitters, makes neural network computations a complicated and intricate topic of study. The operations occurring within and between the individual neurons of neural circuits, have been widely investigated in a neural circuit such as the insect`s antennal lobe (AL; their primary olfactory center). Here, local interneurons (LNs) and projection neurons (PNs) are representative neurons involved in processing olfactory information. By using intracellular recording and iontophoretic staining, the neuromorphology and electrophysiological responses to stimulation has been studied extensively in AL PNs (e.g. Berg, Almaas, Bjaalie, & Mustaparta, 1998; Christensen, Mustaparta, & Hildebrand, 1991; Kanzaki, Arbas, Strausfeld, & Hildebrand, 1989; Zhao et al., 2014), and in LNs (e.g. Chou et al., 2010; Christensen, Waldrop, Harrow, & Hildebrand, 1993; Reisenman, Dacks, & Hildebrand, 2011; Seki & Kanzaki, 2008; Seki, Rybak, Wicher, Sachse, & Hansson, 2010).

Spontaneous spiking activity is the neuron`s activity in the absence of external stimulations. The resting state activity plays an important role of providing a reference context in spiking (Moore, Perkel, & Segundo, 1966). Via regulating the spiking activity in response to stimulation, the communication of stimulation information occurs between pre- and postsynaptic neurons (Christensen et al., 1993; Tabuchi et al., 2015).

1.1. Investigating neural electrophysiological properties

Electrophysiological data can be obtained through either extracellular or intracellular recording. In contrast to the large sample recordings conducted by the extracellular technique, the good contact of a single neuron through a glass microelectrode is more difficult to establish. The advantages of the intracellular recording is that it gives the possibility of observing the physiological activity of an individual neuron, in addition to neuron labelling using fluorescent dye injection. This injected dye facilitates the neuron`s visualization and morphological classification. Several physiological parameters can be used to characterize the recorded activity of the neuron.

1.1.1. The interspike interval

The interspike interval (ISI) is an estimate of the observed length of intervals between spikes, measured in a temporally constricted window. Examples of ISI histograms are shown in Figure 1, this displays the observed count of ISIs of different lengths shorter than 100 ms. In the example figure, these 100 ms were divided into twenty time-bins. The analyst determines the total duration of the ISI histogram and the number of time-bins. The histogram is informative of the distribution of spiking activity (Moore et al., 1966; Perkel, Gerstein, & Moore, 1967). Biphasic distributions, like the Poisson distribution, signifies high spike train irregularity (Nawrot et al., 2008). This could indicate bursty spiking. In contrast, more uniform distributions represent a larger extent of consistent and non-bursty spiking. A bursty firing neuron displays intermittent bursts of spikes followed by hyperpolarization, as opposed to a non-bursty neuron which displays regularly fired spikes (Alving, 1968; Lei, Reisenman, Wilson, Gabbur, & Hildebrand, 2011). Bursting spike strains provide more reliable data than a single spike does, in terms of initiating a response in the postsynaptic neuron (reviewed by Lisman, 1997). Nevertheless, a single synapse would in most instances not be enough to bring a postsynaptic neuron to action potential threshold. However, bursting has also been shown to be associated with synchronization of neural networks (Izhikevich, 2000). During synchronized activity, several neurons can synapse onto a postsynaptic neuron simultaneously (reviewed by Lisman, 1997). This will increase the likelihood of postsynaptic neurons reaching action potential thresholds.

Commonly used parameters based on the ISI include the *ISI mean*, as well as the *ISI coefficient of variance* (cV), i.e. the standard deviation of interval lengths divided by the mean of interval lengths (Nawrot, 2010):

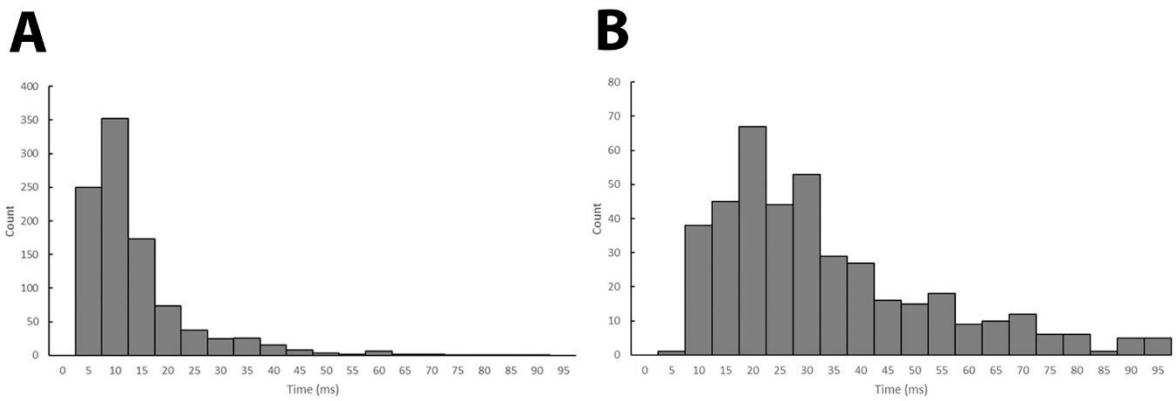

Figure 1. Interspike interval (ISI) histograms, the x-axis shows timelines of 100 ms, split into 20 time-bins, each 5 ms long. The y-axis displays the count of observed ISIs in each time-bin. **A)** An ISI histogram displaying a biphasic, irregular process, taken from a projection neuron (ISI *M* = 49.10, *cV* = 1.96). **B)** ISI histogram for a local interneuron (ISI *M* = 20.35, *cV* = 0.95). This neuron exhibits a Poisson-like distribution.

Equation 1 $$\boldsymbol{cV = \frac{SD(X)}{M(X)}}$$

Where *SD(X)* is the standard deviation of observed ISIs in a neuron, while *M(X)* is the mean of observed intervals. A Poisson process is a distinct instance of a Gamma process, and has an ISI cV = 1 (van Vreeswijk, 2010), which denotes a quite high degree of spike train irregularity. Even higher ISI cV values indicate highly irregular ISI distributions (as in Figure 1 A), possibly represented by a large degree of bursty behavior. Yet, a high ISI cV is not necessarily synonymous with bursty firing. For instance, low firing neurons with large ISI variability and no bursty spiking would have high ISI cV values. Low ISI cV values would be found in regularly spiking neurons with low ISI variability.

1.1.2. Firing frequency

The *spontaneous firing rate* is the mean count of spikes in a series of temporally constricted observation windows. This can be used to calculate thresholds of excitatory and inhibitory responses (e.g. Reisenman et al., 2011), which the spike frequency during stimulation ought to transcend to be classified as a valid or significant response. However, the spontaneous firing rate can also be used as a parameter to characterize physiological activity in the absence of stimulation. This requires stationarity, which implies that the ISIs are random processes uninfluenced by extrinsic factors (Moore et al., 1966). The *Fano Factor* (FF; Fano, 1947), is a parameter quantifying the variability of the firing rate. The FF is provided by the variance of the spike count divided by the mean of the spike count (Nawrot, 2010):

Equation 2 $$\boldsymbol{FF = \frac{Var(n^j)}{M(n^j)}}$$

Where (n^j) is the observed spike count n in a fixed time window being repeated by number of observations j. *Var* is the variance of spike count, and M is the mean spike count. The spontaneous firing rate is a parameter closely related to the ISI mean, while the FF and ISI cV^2 have been reported to be theoretically identical; FF $\propto$ = cV^2 $\propto$ (Nawrot et al., 2008).

1.1.3. Waveforms

Parameters presenting the shape of action potentials (the waveform), can also be used to typify the electrophysiological characteristics of neurons. Parameters describing the duration of the action potential, e.g. the *full-width at half maximum* (FWHM) and the *spike duration* (see Figure 2), are commonly used (e.g. Christensen et al., 1993; Seki et al., 2010; Tabuchi et al., 2015). Differences in spike durations of distinctive neuron categories can be informative of differences in amount of neurotransmitter release. For instance, longer action potentials lead to greater presynaptic influx of calcium (Ca^{2+}), resulting in lengthier exocytosis (Deng et al., 2013; Hochner, Klein, Schacher, & Kandel, 1986).

1.2. Electrophysiological properties of antennal lobe neurons

Local interneurons (Figure 3 A), confined to a small brain region, contains dendrites which can act as both pre- and postsynaptic terminals. Thus, the releasing and receiving of neurotransmitter occur in the same region in this neuron category (Chou et al., 2010). In projection neurons (Figure 3 B), the input dendrites and output terminals are located in different brain regions, indicative of the PN`s ability to convey information between distant neuropils (Yasuyama, Meinertzhagen, & Schürmann, 2002). Comparisons of LN and PN physiology has only been reported by a small number of studies, and to our knowledge, only one study has statistically compared the spontaneous activity of these neuron categories (Lei et al., 2011). The FWHM was observed to be longer in LNs than in PNs (Christensen et al., 1993), while ISI irregularity differed between these two neuron categories (Lei et al., 2011; Meyer, Galizia, & Nawrot, 2013). In the moth *Manduca sexta*, the spontaneous activity of LNs was found to display more regular firing-patterns than PNs. The PNs had significantly higher ISI cV values than LNs, which was caused by bursty firing (Lei et al., 2011). Oppositely, Meyer et al. (2013) found the LNs of *Apis mellifera* to exhibit a higher degree of ISI irregularity than that of the PNs, however they included stimulation data in their measure of ISI cV. Only for LNs, the presence of two sets of spikes has been observed (Christensen, D'Alessandro, Lega, & Hildebrand, 2001; Christensen et al., 1993). The smaller spikes could originate from excitatory postsynaptic potentials (EPSPs) in the dendrites, while the larger

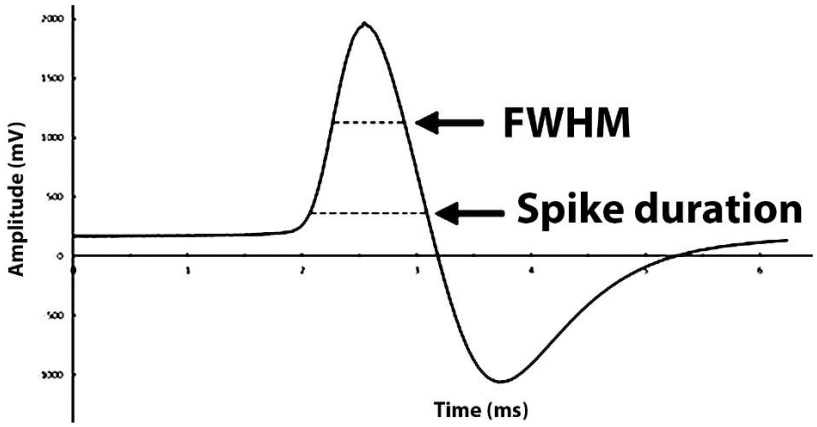

Figure 2. Waveform average displaying the parameters full-width at half maximum (FWHM) and the spike duration. The figure displays the average of all waveforms fitting with a specific wavemark (see section 2.8.1.3.) in a recording. The membrane potential was here amplified tenfold.

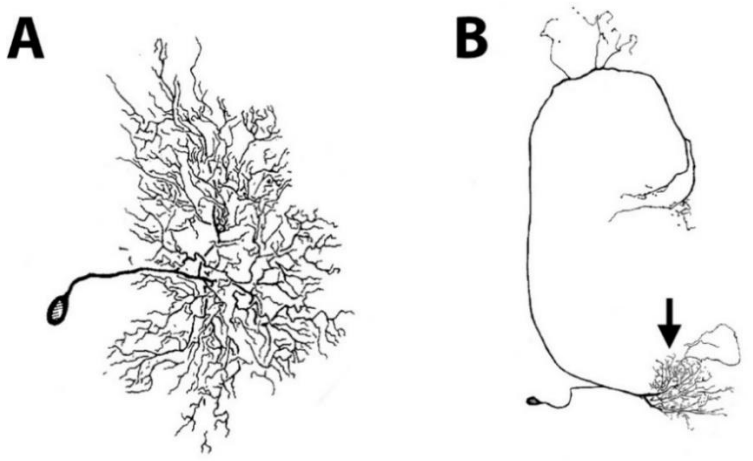

Figure 3. Two different neuron categories. **A)** A unipolar local interneuron (LN), with dendritic arborizations limited to one single region, e.g. the antennal lobe. The LN has no projection axon. **B)** A bipolar projection neuron, the black arrow pointing to dendrites. The axon is seen on the upper end, projecting to distant neuropils. Adapted from Hansson (1995).

spikes could be action potentials from the main neurite (Christensen et al., 2001).

By statistically classifying AL neurons based on spontaneous physiological properties, Lei et al. (2011) correctly classified at most 90% of LNs and PNs in *M. sexta*, as verified by morphological data. In *A. mellifera*, Meyer et al. (2013) classified 90% of LNs and PNs correctly with a cluster analysis, but they used odor responses rather than spontaneous activity.

1.3. Heliothine moths as model organisms

The AL of *Heliothine* moths has frequently been used to study the neuroanatomy of the olfactory pathways (e.g. Berg, Galizia, Brandt, & Mustaparta, 2002; Ian, Berg, Lillevoll, & Berg, 2016a; Ian, Zhao, Lande, & Berg, 2016b; Løfaldli, Kvello, Kirkerud, & Mustaparta,

2012; Rø, Müller, & Mustaparta, 2007; Zhao et al., 2014). However, the electrophysiological characteristics of spontaneous spiking in the PN and LN categories have not been reported upon. Therefore, the moth *Helicoverpa armigera* (*Lepidoptera: Noctuidae, Heliothinae*), is used in this thesis to provide a better understanding of physiological features in these neuron categories. This can allow for a better conception of the encoding of olfactory information in the *Heliothine* brain.

1.4. Olfactory information processing

1.4.1. Sensory transduction and the primary olfactory center

Sensory transduction of odorant molecules occurs inside the sensillae of the antennae, which contains the olfactory sensory neurons (OSNs; reviewed by Mustaparta, 2002). Once inside the sensillum, the odorants are transported to olfactory receptors located on the dendrites of the OSNs by odor binding proteins (e.g. Zhang et al., 2012). A bundle of OSN axons forms the antennal nerve, which carries olfactory information to the AL.

In *H. armigera*, each AL consists of 79 glomeruli (Zhao et al., 2016), which are synaptically dense neuropils processing olfactory information. Glomeruli are convergence points of OSNs, LNs, PNs (reviewed by Galizia & Rössler, 2010) and modulatory centrifugal neurons (CNs; e.g. Zhao, Pfuhl, Surlykke, Tro, & Berg, 2013). In *Drosophila melanogaster*, OSNs which express specific olfactory receptor genes innervates the same glomeruli (Gao, Yuan, & Chess, 2000). Similar structural organization has also been reported in *Heliothine* moths, where OSNs responding to specific pheromones project to the same glomeruli (e.g. Berg et al., 1998). The glomeruli of the male *H. armigera* AL has been classified into four subgroups: the posterior complex (PCx; 10 glomeruli with unknown function), the carbon dioxide responsive (Stange & Wong, 1993) labial-palp pit organ glomerulus (LPOG; one glomerulus), the macroglomerular complex (MGC; three glomeruli) and the ordinary glomeruli (OG; 65 glomeruli) (Zhao et al., 2016). The MGC has been shown to be pheromone sensitive in several studies (e.g. Berg et al., 1998; Galizia, Sachse, & Mustaparta, 2000; Wu et al., 2015). It consists of the cumulus, the largest MGC glomerulus, along with the anterior dorso-medial unit (dm-a) and the posterior dorso-medial unit (dm-p) (Zhao et al., 2016). The cumulus is responsive to the intraspecific primary pheromone component, *cis*-11-hexadecenal (Z11-16:AL), while the dm-p responds to the secondary pheromone component, *cis*-9-hexadecenal (Z9-16:AL). Both components are agonists of sexual behavior in this species. Interspecific component *cis*-9-tetradecenal (Z9-14:AL) operates as an antagonist of sexual behavior (Kehat & Dunkelblum, 1990), and is processed in the dm-a and the dm-p (Wu et al.,

2015). The OG process general odorants, such as host-plant odorants (reviewed by Mustaparta, 2002). Somata of LNs and PNs are found in three AL cell clusters; the lateral, anterior and medial cell body clusters (LCC, ACC and MCC, respectively; Homberg, Montague, & Hildebrand, 1988).

1.4.2. Projection neurons of the antennal lobe tracts

In moths, the output from the AL is projected towards third order odor neurons in the protocerebrum primarily through three main antennal lobe tracts (ALTs). These are the medial (mALT), mediolateral (mlALT) and lateral (lALT) tracts (see Figure 4; Homberg et al., 1988; Ian et al., 2016b; Rø et al., 2007), which are also found in most other insect species (Ito et al., 2014).

The mALT mainly consists of PNs with uniglomerular innervations. The axons of mALT PNs project posteriorly to the calyces of the mushroom bodies (MBs), which are involved in associative odor-memory consolidation and retrieval (e.g. Akalal, Yu, & Davis, 2010; De Belle & Heisenberg, 1994). There are two calyces in each brain-hemisphere; the medial and the lateral calyx, which contains the dendrites of Kenyon cells (MB neurons). The PN output terminals of several ALTs overlap with dendrites of Kenyon cells (Rø et al., 2007). From the calyces, the mALT axons projects to the lateral protocerebrum. Here, innervated neuropils may include one or several regions listed below: The lateral horn (LH), ventro-medial neuropil (VMNP), inferior neuropil (INP), superior neuropil (SNP), anterior ventro-lateral protocerebrum (AVLP) and the postero-lateral protocerebrum (PLP) (Ian et al., 2016b; Figure 5). Both AL PNs and sensory neurons from other modalities innervate lateral protocerebral regions in *Heliothinae*. The AVLP, for instance, is innervated by AL PNs (Ian et al., 2016b), in addition to auditory ventral-cord neurons (Pfuhl, Zhao, Ian, Surlykke, & Berg, 2014). The LH has also been linked with experience-independent odor behaviors (reviewed by Masse, Turner, & Jefferis, 2009). Reportedly, medial-tract PNs innervating the OG and the MGC have dissimilar protocerebral innervation patterns in the calyces. The OG mALT neurons innervate large portions of the calyces, while interspecific MGC medial-tract neurons innervate the inner areas of the calyces (Zhao et al., 2014).

The mediolateral ALT PNs projects postero-laterally to the lateral protocerebrum, where they terminate in the LH, SNP and PLP (Ian et al., 2016b), avoiding the calyces. Several studies have reported mlALT neurons to be strictly multiglomerular, and somata are generally located in the LCC (e.g. Homberg et al., 1988; Rø et al., 2007).

The lateral-tract, which contains both uni- and multiglomerular neurons, projects

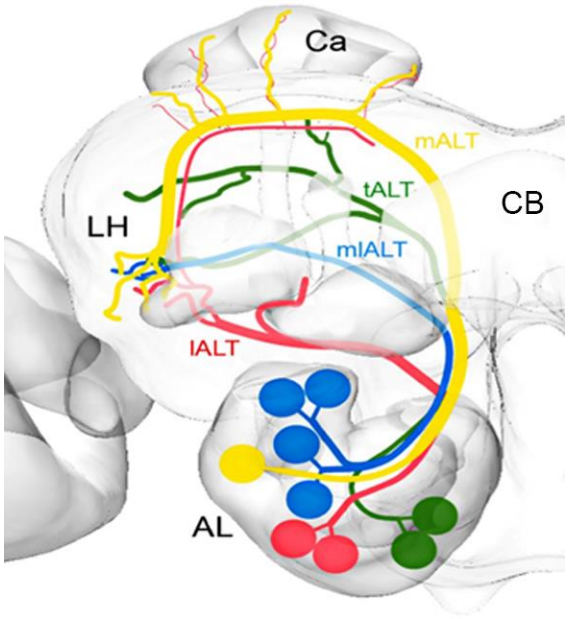

Figure 4. Illustration of antennal lobe tracts (ALTs), in dorsal view. The yellow medial ALT (mALT) has one glomerulus, due to mainly uniglomerular innervations. The blue mediolateral ALT (mlALT) shows four glomeruli, due to multiglomerular innervations. The red lateral ALT (lALT) and the green transverse ALT (tALT) has two glomeruli, signifying both uni- and multiglomerular neurons. AL - antennal lobe; Ca - calyces of the mushroom body; CB – central body; LH - lateral horn. Figure adapted from Ian et al. (2016a).

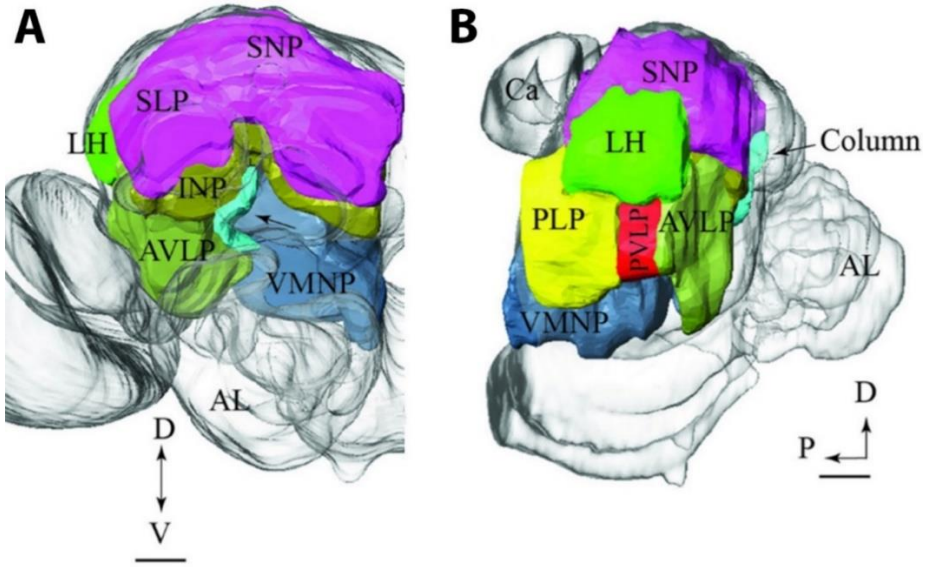

Figure 5. Protocerebral neuropils displayed from **A)** fronto-dorsal view, and **B)** at a sagittal view. Black arrows point at the column. AL – antennal lobe; AVLP – anterior ventro-lateral protocerebrum; Ca – calyces of the mushroom bodies; INP – inferior neuropil; LH – lateral horn; PLP – posterior lateral protocerebrum; PVLP – posterior ventro-lateral protocerebrum; SLP – superior lateral protocerebrum; SNP – superior neuropil; VMNP – ventro-medial neuropil. Scale bars: 50 μm. Adapted from Ian et al. (2016b).

dorso-laterally from the AL, and runs postero-laterally towards lateral protocerebral neuropils. Numerous subcategories of lALT neurons have been identified, due to the tract`s heterogeneous branching patterns (Ian et al., 2016b). Innervated neuropils includes the LH,

AVLP, PVLP, SNP, INP and the newly discovered *column* (see Figure 5; Ian et al., 2016b). A few lALT PNs have been found to project postero-medially to the calyces after innervating the lateral protocerebrum (Homberg et al., 1988; Ian et al., 2016b).

A tract termed the transverse ALT (tALT) was recently discovered in *Heliothis virescens* (Ian et al., 2016a). The tALT exits the AL medially, alongside the mALT and mlALT, and continues posteriorly until the posterior side of the central body. Mass stains has shown that the axons split at this point. One sub-branch bends antero-laterally to innervate the LH, then turns postero-medially to innervate the base of the medial calyx. The second sub-branch innervates the medial calyx and the posterior lateral protocerebrum (Ian et al., 2016a).

1.4.3. Local interneurons characteristics

In the cockroach *Periplaneta Americana* (Watanabe, Ai, & Yokohari, 2012), the honeybee *A. Mellifera* (Stopfer, Bhagavan, Smith, & Laurent, 1997), and the moth *M. sexta* (Lei, Christensen, & Hildebrand, 2002, 2004), LNs have been shown to enable synchronized activity across glomeruli. Such synchronized activity is associated with reliable output (reviewed by Lisman, 1997). For the AL neural network, this includes synchronizing PN burstiness. The LNs can interact with AL PNs, OSNs and other LNs by means of interglomerular lateral inhibition and disinhibition (Christensen et al., 1993; Tabuchi et al., 2015; Wilson & Laurent, 2005), global AL inhibition (Silbering & Galizia, 2007) and lateral excitation (Shang, Claridge-Chang, Sjulson, Pypaert, & Miesenböck, 2007). *Lateral* here refers to mediation of adjacent neurons. These mechanisms provides gain control, increasing PN responsiveness to weak stimulations, while reducing PN sensitivity during strong odorant stimulations (reviewed by Masse et al., 2009). Insect LNs hold a variety of neurotransmitters. Some LNs use inhibitory GABA (γ-aminobutyric acid; Berg, Schachtner, & Homberg, 2009; Chou et al., 2010; Reisenman et al., 2011) while others use excitatory acetylcholine, dopamine or glutamine (Chou et al., 2010; Shang et al., 2007) to interact with AL neurons.

The LNs, confined to the AL, are quite morphologically heterogeneous. LNs has been categorized as panglomerular (innervating all glomeruli), multiglomerular with symmetric/asymmetric dendritic density, and oligoglomerular, i.e. targeting only a few glomeruli (Chou et al., 2010; Seki & Kanzaki, 2008; Tabuchi et al., 2015). It is reported that all AL LNs have their somata in the LCC (e.g. Berg et al., 2009; Matsumoto & Hildebrand, 1981). For panglomerular LNs, a primary neurite ordinarily extends towards the antennal lobe hub (an aglomerular region at the core of the AL, containing branches of PNs and LNs), then thinner neurites radiate out into the glomeruli.

1.5. Aims of the thesis.

Since characterization of spontaneous activity in LNs and PNs have received little attention, the main aim of this thesis is to characterize and investigate putative differences in the spontaneous spiking patterns of LN and PN categories. Specifically, physiological parameters related to the spontaneous spiking in these respective neuron categories will be used in an attempt to classify neuron type without including neuron category into the analyses. Subsequently, physiological classifications are to be compared to morphological classifications. In addition, individual physiological parameters will be investigated for potential differences between LNs and PNs. To this end, the experimental method of intracellular recording and iontophoretic staining of individual AL neurons will be performed. The anatomical data will be analyzed via confocal microscopy and the electrophysiological via statistical analysis. The secondary aim is to investigate whether distinct PN categories can be characterized by their spontaneous activity. Information on putative physiological differences between separate AL neuron types can be conducive to future research as such distinctions might contribute to identification of specific neuron categories already during the recording experiments. A tertiary aim of this thesis is to identify any recorded AL neuron morphologically, including PNs confined to distinct AL-tracts and LNs displaying varied branching patterns.

2. Materials and methods

2.1. Experimental subjects

Male moths of the species *Helicoverpa armigera* (*Lepidoptera; Noctuidae, Heliothinae*) were used as experimental subjects. Pupae of the moths were purchased from China (Henan Jiyuan Baiyun Industry Co., Ltd). The pupae were kept in climate chambers (Refritherm 200 and 6E, Struers-Kebolab, Albertsund, Denmark, or Binder KBF 720, Tuttlingen, Germany) at 23°C and 70% air humidity. A reversed night-day cycle was used, with 14 hours light and 10 hours dark.

Two housing conditions were provided to the moths. In a classic housing condition, up to eight emerged moths were placed into cylindrical Plexiglas containers (diameter 12.5 cm, height 20 cm). These fed on 10% sucrose solution stationed at the base of the container. Papers were taped on the cylinder`s walls, allowing the moths to climb. In addition, an unconventional semi-natural housing condition was applied. At most 25 pupae were placed in large Plexiglas containers (diameter 29 cm, height 40 cm), with mesh lids. Upon emergence, the moths fed on sucrose solution paired with 40 µl sunflower abstract (from sunflower leaves, *Helianthus annuus*) applied to a circular filter paper (diameter 1.5 cm). These were attached 33 cm high up on the container, requiring the moths to fly in order to feed.

2.2. Preparation of experimental odorants

Six stimuli were applied during intracellular recording (four pheromone compounds, one control and one plant odor). All stimulations were given at a volume of 20 µl. However, all pheromone stimuli were diluted in hexane with a final concentration 50 ng/ 100 µl. Hexane also served as the control stimulus to eliminate mechanosensory responses. A plant odor, the sunflower abstract, was not diluted. We used a two-component intraspecific pheromone blend, i.e., the primary (*cis*-11-hexadecenal; Z11-16:AL) and secondary (*cis*-9-hexadecenal; Z9-16:AL) pheromones in a 95:5 ratio (Pheromone chemicals, Plant Research International, Pherobank, Wageningen, Netherlands). Additionally, the constituents of the pheromone blend were tested individually. An interspecific pheromone, *cis*-9-tetradecenal (Z9-14:AL), was also used. The odorants were applied to a small piece of clean filter paper inside a glass cartridge (inner diameter 0.4 cm). When not in use, the odorants were sealed and stored in a freezer at -18°C. The odor stimuli were regularly renewed during the experimental period.

2.3. Preparation of insects

After being kept in a refrigerator for about 10 minutes at 4°C for pacification, a moth was placed inside a plastic tube. Only the head was displayed. Under a stereomicroscope

(Leica, M60), dental wax (Kerr Corporation, Romulus, MI, USA) was carefully applied around the compound eyes and the neck to immobilize the moth (Figure 6 A), preventing disruptive movements during intracellular recording. The cephalic scales covering the head were gently removed to expose the head capsule. Part of the cuticle covering the brain was cut off with a razor knife. Trachea covering the antennal lobes and protocerebral regions were removed using fine forcipes. The nerve connecting intracranial muscles and the antennae was removed using forcipes, however removal was not achieved for all preparations. Whenever necessary, Ringer`s solution with sucrose (NaCl: 150 mM, KCl: 3mM, TES buffer: 10 MM, $CaCl_2$: 3mM, sucrose: 25 mM, pH: 6.9) was applied using a syringe, to prevent desiccation.

2.4. Intracellular recording

After preparation, the moth was mounted under a microscope (Leica MZ Apo). This was stationed on a laboratory table (Micro-G, Technical Manufacturing Corporation, Peabody, MA, USA) inside a Faraday cage. A silver-nitrate coated silver-wire was placed anteriorly in the mouth muscle. It served as a reference electrode and aided in constricting movement of the head. A borosilicate glass microelectrode was pulled using a Flaming-Brown horizontal puller (P97; Sutter instruments, Novato, CA, USA). Dextran tetramethylrhodamine-biotin (Micro-ruby, Life Technologies, USA), a fluorescent dye, was filled in the tip of the microelectrode. Subsequently, potassium acetate (0.2 M) was back-filled into the microelectrode using a small syringe. The dye-filled microelectrode was attached to a silver wire joined to a head-stage preamplifier (HS-2, Axon instruments, USA). This was connected to an amplifier (Axoprobe-1A, Axon instruments, USA). These electrodes ensured a current circuitry, measuring voltage fluctuations between the recording and reference electrodes.

The recording electrode was then inserted into an antennal lobe (Figure 6 B) using a micromanipulator (Leica). The voltage fluctuations were displayed on an oscilloscope (Tektronix 5111A, Oregon, USA). A Micro 1401 mkII data acquisition unit (Cambridge Electronic Design Limited, Cambridge, UK) digitalized these signals, allowing a connected computer to record and display voltage fluctuations using a custom written script in the software Spike2 (version 6.14, Cambridge Electronic Design Limited). Action potentials also provided a crisp and distinct sound, provided by a loud-speaker (Monacor, MAB-30AK) connected to the amplifier.

2.5. Stimulation and iontophoretic staining

The Spike2 script contained stimulation codes and allowed for iontophoretic staining

of a contacted neuron through the amplifier sending current pulses. A continuous air flow (500 ml/min) was directed at the antenna ipsilaterally positioned to the contacted AL through a Teflon tube. This air flow was applied to remove remnants of odorant molecules. The glass cartridges containing experimental odorants were one by one attached to a second Teflon tube, and positioned ~1 cm from the antenna in parallel with the continuous air flow. The odorants were administered by command in Spike2, through a mechanical valve system. This command initiated a 500 ml/min air flow lasting for 400 ms.

All six stimuli were ordinarily applied three times, for a total of 18 stimulations. The time interval between stimulations was usually 8-15 seconds. A subjective assessment by the experimenter decided whether the contacted neuron appeared to demonstrate odor responsiveness. Responsive and stably contacted neurons were stained with either a 2 nA hyperpolarizing current pulse for approximately 20 minutes, or a 3 nA depolarizing current pulse (200 ms, 2Hz) for 10-15 minutes. Post-staining resistance of the recording electrode was generally in the range of 70-350 MΩ.

2.6. Dissection, fixation, and dehydration

After staining, the moth was placed in a sealed container, and kept in a refrigerator (4°C) for 12-24 hours. This allowed the dye to get distributed throughout the neuron via axoplasmic transport. Afterwards, the moth was placed under a stereomicroscope (Leica, M60) for dissection. The antennae, labial palps and proboscis were cut off using microscissors, and compound eyes were removed using a razor knife and forcipes. The moths head was detached and the brain was carefully dissected out, by removing the remainder of the cuticle and trachea using forcipes. After dissection, the brain was fixated in 4% paraformaldehyde (Roti-Histofix 4%, Carl Roth GmbH, Karlsruhe, Germany) for one hour in room temperature. Then, the brain was dehydrated in an ascending ethanol series (50, 70, 90, 96 and 2 × 100%, 10 minutes each). Finally, the brain was made transparent in methyl salicylate (methyl 2-hydroxybenzonate) and put between two cover glass slides placed on a 1 mm thick aluminum plate, ready for confocal imaging.

2.7. Confocal microscopy imaging

After an initial check in a light microscope (Leica, DMC 4500), the aluminum plates containing the preparations were brought to the Department of Biophysics and Medical Technology, NTNU. The brains were imaged there, using a confocal laser scanning microscope (Zeiss LSM 800, Jena, Germany). Brains were visualized using a 10x (C-Apochromat 10x/0.45 NA) water lens objective, or a 20x (Plan Neofluar 20x/0.5 NA) dry lens

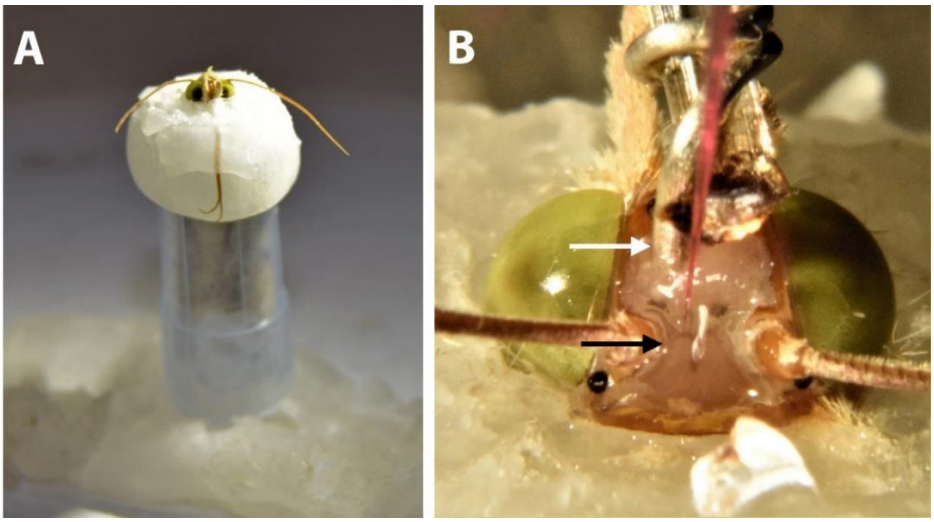

Figure 6. Data gathering through intracellular recording and iontophoretic staining. **A)** Image displaying a moth immobilized inside a plastic tube. **B)** Image of intracellular recording. The black arrow indicates the antennal lobe, where the glass microelectrode had been inserted. The white arrow indicates the reference electrode, which only in this instance was coiled around an optical fiber, allowing effective illumination of the brain.

objective. For scanning, one channel with a helium-neon laser at 561 nm wavelength excited the micro-ruby, while a second channel used an argon laser at 488 nm wavelength excited auto-fluorescent molecules to visualize the brain. A resolution of 1024 x 1024 pixels was used for all preparations. The pinhole size was set to 1 airy unit. Slices was between 4-10 μm, giving slice overlap in the range of 5-50%. Low slice overlap would reduce the scanning time, thus preserving the brain from lasing bleaching while still providing scans of satisfactory quality. The images were acquired and processed using the software ZEN 2 (blue edition, Carl Zeiss Microscopy GmbH, Jena, Germany).

2.8. Data analysis

2.8.1. Preliminary analyses

Images from confocal microscopy were used to classify stained neurons. Only preparations where stained neurons could be classified as AL PNs, or AL LNs were included for further analyses. In preparations where more than one neuron was clearly stained, the morphology of the stained neurons would have to be homogenous to be included, and waveforms had to be of approximately the same duration. The AL neurons were classified by cell cluster and glomerular arborizations, projection neurons were additionally classified according to which ALT they projected in.

The electrophysiological data went through a preliminary inspection, in which stimulations containing manual noise or less than five seconds between stimulations were removed. Observation periods were set to 4000 ms. The initial 1000 ms were defined as the

pre-stimulation window, followed by 400 ms of stimulation, and a 2600 ms post-stimulation window. To ensure a constant bias in data removal during stimulation trains, two heuristics were used for all removals: 1, only overlapping stimulation windows or manual noise led to deletion of stimulations, 2, if one out of two stimulations had to be deleted, the earliest stimulation would be deleted. Additionally, intracellular recordings containing less than five valid stimulations would be excluded from all analyses of electrophysiology.

2.8.2. Spike sorting

Separating neural signal from noise was performed using the Wavemark tool in Spike2. Wavemark templates were created based on the recorded waveforms, only wavemarks fitting waveforms of action potentials were utilized. Wavemarks from minor membrane fluctuations were discarded by altering wavemark inclusion thresholds. In recordings with more than one wavemark, the similarity of waveforms was compared by filtering the wavemarks, and then checking waveform averages for each of the wavemarks. If the difference in spike durations was less than 1 ms, the spike amplitudes were comparable and the morphologies of stained neurons were homogenous, the wavemarks would be merged. All recorded waveforms fitting the wavemark would be indicated as an event, all events were applicable to further analyses.

2.8.3. Interval and frequency parameters

To quantify the ISIs during the spontaneous activity of a given neuron, the 1000 ms pre-stimulation windows were employed. Using the Interval histogram tool in Spike2, ISI histograms were created to show the distribution of time-intervals between spikes. The x-axis of the ISI histogram had a timeline of 100 ms, split into 20 time-bins, each 5 ms long, while the y-axis displayed the count of observed interspike intervals in these time-bins. The data from the ISI histograms were saved as text files, for ensuing use in statistical analyses. The parameters extracted from these were the ISI mean, as well as the ISI cV (see Equation 1).

The Peri-stimulus histogram (PSTH) tool in Spike2 was used to quantify the frequency of spikes in the spontaneous activity of neurons, as measured in the 1000 ms pre-stimulation windows. PSTHs were saved as text files, and exported to Microsoft Excel. These data were used to calculate the spontaneous firing rate, which is the mean count of spikes in the pre-stimulation period across all trials, as well as the FF (Equation 2).

2.8.4. Waveform parameters

The FWHM and the spike duration, both in ms, were assessed using the Waveform

average tool in Spike2. The average waveform, containing amplitude along a time-axis, was exported into Excel as a text file. Here, the time-point of largest amplitude increase could be identified. This time-point would indicate action potential threshold. The spike duration was defined as the duration between the transmembrane potential reaching action potential threshold during depolarization, until the time at which the membrane potential reached the equivalent amplitude during repolarization. For the parameter FWHM, the equidistant point between action potential threshold and maximum amplitude was first identified. The FWHM was then defined as the duration between the upward and downward slopes at this amplitude (see Figure 2).

2.8.5. Odor response characteristics

Visual inspection of Spike2 recordings and PSTHs were performed to assess responses to odor stimulation. Inspection of responses without quantitative thresholds have been used in numerous studies on odor responses (e.g. Berg et al., 1998; Zhao et al., 2014). A response was classified as excitatory if the spike frequency increased substantially and reliably in all trials with the same stimulus. An inhibitory response was defined by a reliable cessation of spiking throughout the stimulation window. The definition of a complex response required both excitation and inhibition within the same stimulation window.

2.9. Statistical analyses

Using the physiological parameters extracted (Table 1) for LNs and PNs, an unsupervised two-step cluster analysis (Schwarz's Bayesian criterion with log likelihood distance) was performed in SPSS (Version 24.0), The ISI mean and ISI cV were used to quantify spike timing and spike-time irregularity, while the spontaneous firing rate and the FF were used to quantify firing frequency and firing frequency variability. The FWHM and the spike duration were used to quantify the action potential duration. If the quality of the cluster analysis was better than "fair", it was followed up with a *chi-square* test to compare the difference between the cluster result and the morphological classification (LN or PN). The goodness-of-fit between these two was reported. Due to concerns regarding the assumption of independence (parameters should not be highly correlated), an additional cluster analysis was performed to investigate classification performance when controlling for collinearity.

The same analyses were performed using only the data from the PNs. Two PN features were candidates for comparisons between this cluster result and morphology: PN tract and dendritic arborizations. For PN tract, we set PNs in mALT as Group mALT and PNs in other ALTs as Group oALTs. According to the different dendritic arborizations, we set PNs

Table 1

List of all variables used for cluster analyses of spontaneous activity.

Interspike interval mean
Interspike interval coefficient of variation (cV)
Spontaneous firing rate
Spontaneous firing rate fano factor (FF)
Full-width at half maximum (FWHM)
Spike duration

innervating only one glomerulus as Group UG as well as PNs innervating several glomeruli as Group MG. *Cramer`s V* was reported as an effect size for the *Chi-square* analyses. As this effect size is associated with *Pearson`s correlation coefficient* (reviewed by Ferguson, 2009), it is appropriate to use the same effect size benchmarks as for *r*. Accordingly, *Cramer`s V* = .1, = .3, and = .5 constitutes small, medium and large effects, respectively (Cohen, 1992).

Differences in parameter values between neuron categories were inspected with box-plots and descriptive statistics. For parameters with noteworthy differences between neuron categories, non-parametric *Mann-Whitney U-tests* were performed to check whether such differences might be significant. In addition, differences in ISI distributions of neuron categories were investigated using three mixed-design *analyses of variance* (*mixed ANOVAs*) in JASP (JASP TEAM, version 0.8.1.1). The *mixed ANOVA* combines repeated-measures and between-group effects. There were two factors, one of which was time separated into twenty time-bins, the other was neuron category. The neuron category was different for each of the analyses, one was grouped by LNs or PNs, the second by mALT or the other ALTs pooled, the third was grouped by uniglomerular or multiglomerular PNs. All reported probabilities were two-tailed and asymptotic.

2.10. Ethical considerations

None of the requirements described in *Regulation for use of animals in research trials* (Forskrift om bruk av dyr i forsøk, 2015) included *Lepidopteran* species. Nevertheless, precautions were made to ensure the welfare of the moths. They were cared for daily, this care included sucrose provision and changing of soiled papers inside their housing containers. In the unconventional housing condition, the moths were required to fly in order to feed. The relatively spacious cylinders used, allowed for a higher freedom of movement than in the classical housing condition.

3. Results

In total, 148 moths were used for experimental purposes in this thesis. Of these, 73 preparations were stained, among which 28 contained neurons which were classifiable as either AL PNs limited to one tract or LNs. This implies a success rate of 38% (41% counting all individually stained neurons). Five of these 28 preparations were excluded from statistical analyses, in accordance with the exclusion criteria (see section 2.8.1.), leaving 23 for inclusion in the quantitative analyses[1]. The 28 AL preparations either held only one labelled neuron, or two to three homogenous neurons, except for one LN preparation (see section 3.2.5.). For the sake of simplicity, all neurons in any one preparation will henceforth be analyzed and referred to as one neuron, unless otherwise noted. In addition, 11 other preparations (see appendix Table A1) were also interesting, although not appropriate for the aims of this thesis. An overview of response characteristics of the labelled AL neurons is found in appendix D. In this thesis, the different housing conditions were not part of any analyses.

3.1. Electrophysiological characteristics and cluster analyses

3.1.1. Local interneurons and projection neurons

Using all six physiological parameters (see Table 1; parameter values of individual neurons in appendix Table E1), a two-step cluster analysis without a pre-specified number of clusters (maximum clusters set to 15) converged on two clusters. The cluster quality was "fair", in respect to cohesion and separation. The rank of importance with respect to the physiological parameters was, in descending order: ISI mean, spike duration, spontaneous firing rate, FWHM, FF and ISI cV. A *chi-square* analysis was performed to assess goodness-of-fit. There was a significant association between clustering based on physiological parameters of LNs (N = 10) and PNs (N = 36) with the morphological classification of neuron category, χ^2 (1, N = 46) = 6.35, p = .01, the effect size *Cramer`s V* = .37, was moderate. Cluster 1 consisted of 54% PNs and 46% LNs, while cluster 2 had 88% PNs and 12% LNs. Compared to morphological classification, correct grouping based on physiology occurred for 60% of the LNs and 80% of the PNs, yielding a total correct grouping for 76% of the neurons. Additionally, a cluster analysis was performed utilizing only three parameters, i.e. the spontaneous firing rate, the FF, and spike duration. Here, two clusters were identified, cluster quality was "good", in regard to cohesion and separation. Rank of importance in descending

[1] In addition, Xi Chu also gathered 23 AL neurons (16 PNs, 7 LNs, see appendix table B1) which were included in the statistical analyses presented here.

order was: spike duration, spontaneous firing rate, and FF. The cluster analysis was followed up with a *chi-square* analysis, confirming a significant association of assigned clusters and morphological classification, χ^2 (1, N = 46) = 6.35, p = .01, *Cramer's V* = .37. Cluster 1 had 54% PNs and 46% LNs, while cluster 2 had 88% PNs and 12% LNs. Correct classification was found for 80% of PNs, and 60% of LNs, the total correct classification was 76%. These results were identical to those of the first cluster analysis, indicating that adding the ISI mean, ISI cV and FWHM offered little to the classification performance.

Inspection of box-plots and descriptive statistics indicated no major differences between PNs and LNs with regard to the ISI cV, FF or FWHM (see Table 2 for descriptive statistics). The ISI mean, spontaneous firing rate and spike duration had the largest differences in medians between these neuron categories. The differences in mean ranks of these parameters were non-significant, $p > .05$, as tested by *Mann-Whitney U-tests*. In Figure 7, the averaged ISI distributions of the LN and PN categories are displayed. A *mixed ANOVA* was performed to investigate whether these distributions were significantly different. *Mauchley`s test of sphericity* demonstrated that the assumption of sphericity had been broken ($p < .001$), the *Greenhouse Geisser* correction for degrees of freedom was thus reported. The interaction of time-bins and neuron category was non-significant F (2.24, 98.57) = 0.53, p = .61. This implies that there were no differences in ISI distributions for the LNs and PNs.

3.1.2. Projection neuron categories

Additional two-step cluster analyses were performed to investigate potential sub-categories of PNs. First, we used six physiological parameters, then only three: the spontaneous firing rate, FF and spike duration. Again, using six parameters offered nothing additional to the cluster solution, as such we report only the cluster analysis using three parameters. Two clusters were identified, with the quality of cohesion and separation branded "good". To clarify whether the clusters could be related to morphologically distinct sub-types of PNs, the physiological parameters of the neurons were compared with two morphological features: PNs in different tracts (Group mALT versus Group oALTs) and PNs with different dendritic innervations (uniglomerular versus multiglomerular PNs). According to *chi-square* analysis, there was no significant fit with Group mALT (N = 23) and Group oALTs (N = 12), χ^2 (1, N = 35) = .40, p = .53. Similarly, the identified clusters did not match dendritic arborizations, defined as uniglomerular (N = 19) or multiglomerular (N = 13), χ^2 (1, N = 32) = .39, p = .53. This indicated that the clusters were not attributable to any of these two features.

Table 2

Descriptive statistics for independent variables regarding physiological features

	N	ISI mean	ISI cV	Sp. Firing rate	FF	FWHM	Spike dur.
PN	36	18.18 (13.44) 15.92	0.96 (0.30) 0.91	18.17 (10.19) 17.06	1.41 (1.69) 0.91	0.62 (0.30) 0.49	1.16 (0.57) 0.87
LN	10	20.00 (16.22) 12.92	1.07 (0.36) 1.04	24.28 (14.68) 19.26	1.68 (2.70) 0.63	0.96 (0.79) 0.70	1.80 (1.33) 1.48
mALT	23	19.90 (14.29) 16.55	0.98 (0.30) 0.95	18.90 (10.60) 17.67	1.30 (1.21) 0.94	0.68 (0.32) 0.58	1.28 (0.62) 1.09
Other ALTs	12	15.95 (11.84) 14.50	0.94 (0.31) 0.88	17.56 (9.79) 18.56	1.61 (2.46) 0.68	0.53 (0.24) 0.45	0.96 (0.43) 0.79
UG	19	22.63 (15.28) 18.75	1.02 (0.31) 0.96	21.65 (11.03) 20.74	1.39 (1.97) 0.89	0.65 (0.29) 0.55	1.20 (0.58) 0.97
MG	13	13.07 (9.21) 10.15	0.89 (0.25) 0.88	14.06 (8.34) 11.72	1.37 (1.48) 0.85	0.64 (0.35) 0.47	1.20 (0.63) 0.84

Notes: Means with standard deviations in parentheses, median presented below.
Abbreviations: FF – Fano factor; FWHM – full-width at half maximum; ISI cV – inter-spike interval coefficient of variation; ISI mean – inter-spike interval mean; LN – local interneuron; mALT – medial antennal lobe tract; MG – multiglomerular; Other ALTs – all recorded antennal lobe tracts except the mALT; PN – projection neuron; Spike dur. – spike duration; Sp. Firing rate – spontaneous firing rate; UG – uniglomerular.

The most notable distinction for the ALT partition was in spike duration, for which the Group mALT (*Mdn* = 1.09, *N* = 23) had a significantly higher mean rank than Group oALTs (*Mdn* = 0.79, *N* = 12), *U* = 77.00, *p* = .03, *r* = .36. Also, the mean rank of uniglomerular PNs (*Mdn* = 20.74, *N* = 19) was significantly higher than that of multiglomerular PNs (*Mdn* = 11.72, *N* = 13) concerning the dependent variable spontaneous firing rate, *U* = 71.00, *p* = .04, *r* = .36. Both effect sizes (i.e. *Pearson`s r*) were moderate.

In Figure 8 A, averaged ISI distributions are shown for Group mALT and Group oALTs, while Figure 8 B displays averaged ISI histograms for uni- and multiglomerular PNs. *Mixed ANOVAs* were performed to investigate the ISI distributions according to the confinement to mALT versus oALTs and to uni- versus multiglomerular arborizations patterns. Again, *Mauchley`s test of sphericity* established that the assumption of sphericity had been violated for these analyses ($p < .001$), *Greenhouse Geisser* corrections were thus applied. Both the interaction of time and ALT groups (F (1.89, 62.51) = 1.23, p = .30, as well as time and glomerular innervations (F (1.92, 57.48) = 2.25, p = .12), were non-significant. This implied that the ISI distributions were not significantly different neither in PNs confined

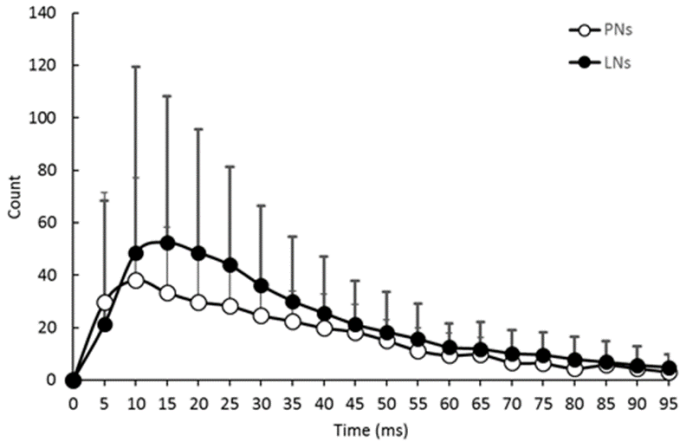

Figure 7. Averaged interspike intervals (ISIs). All local interneurons (LNs) and projection neurons (PNs) were pooled together by category, showing the average ISI distributions of both neuron categories. The error bars represent standard deviations. The x-axis displays 100 ms divided into 20 time-bins, while the y-axis shows average count of ISIs.

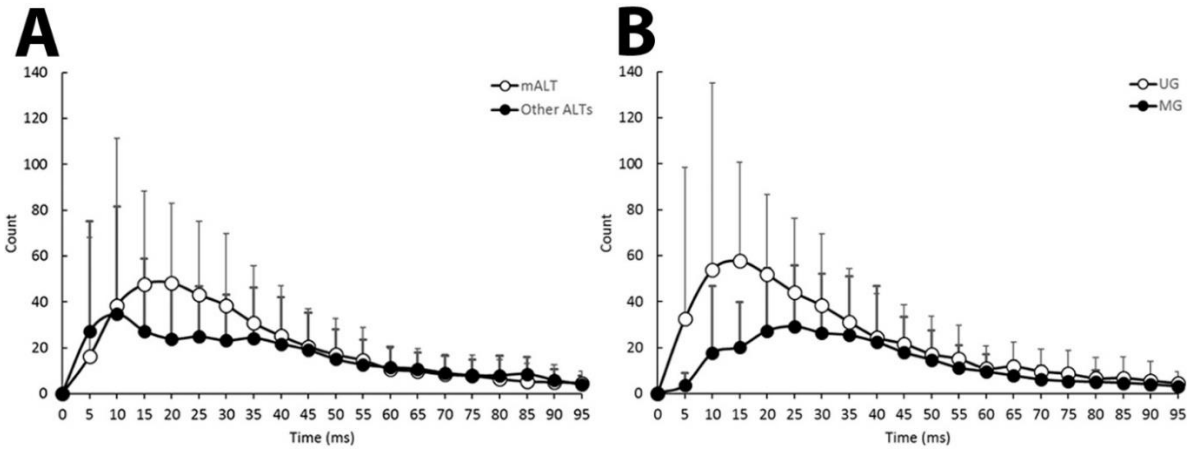

Figure 8. Averaged interspike intervals (ISIs) for projection neuron (PN) categories. **A**) Displays the averaged ISI distributions of medial-tract (mALT) PNs and the remaining tracts (Other ALTs) pooled together. **B**) The averaged ISIs for uni- (UG) and multiglomerular (MG) PNs. Error bars indicate standard deviations.

to the mALT versus oALT nor in the PNs displaying uni- versus multiglomerular arborizations.

3.2. Morphological findings

3.2.1. Medial antennal lobe tract neurons

In all, 14 mALT PNs were stained (all PNs morphologies in Table 3), without additional neuron categories visualized in the same preparations. Somata were found in all cell clusters (see cell clusters in Figure 9 A, E). The majority of medial tract PNs, i.e. nine, were uniglomerular whereas the remaining five were multiglomerular. Four mALT PNs had dendrites in the MGC (see Figure 9 D; appendix figure C1 C and D), whereas three neurons

contained dendrites in PCx glomeruli. The remaining neurons innervated OGs, or had poorly visualized dendrites.

The mALT axons exited the AL close to the midline, running posteriorly to the calyces. The neurons innervated both the medial and lateral calyx, yet the density, thickness and number of axon terminals differed according to glomerular innervations. MGC PNs had sparse innervations, primarily in the inner parts the calyces (see Figure 9 C; appendix Figure C1 C), while OG PNs innervated larger parts more heavily (see Figure 9 A, B; appendix Figure C1 A, B). From the calyces, the axon of all PNs turned antero-laterally, however the innervation patterns in the lateral protocerebrum were somewhat heterogeneous. Specifically, mALT PNs originating from the MGC terminated in a region distinct from that innervated by most neurons linked to OG. PNs from the Cumulus, for example, terminated primarily in medial protocerebral neuropils, such as the SNP, while OG PNs usually only innervated the LH and AVLP.

3.2.2. Lateral antennal lobe tract neurons

Five lALT PNs were stained, of which three were multiglomerular and one uniglomerular, while one neuron`s dendrites and soma were not clearly visualized. The remaining four PNs had somata in the lateral cell cluster. As previously noted by Homberg et al. (1988) and Ian et al. (2016b), the protocerebral projection patterns of lateral-tract PNs were rather heterogeneous (see projection terminals in Table 3; Figures 10 and 11). The lALT neurons innervated various protocerebral regions, including the LH, AVLP, VMNP, and INP.

In Figure 11, an atypical panglomerular PN, innervating all glomeruli, is presented. A neurite left the AL, yet it did not project to the lateral protocerebral neuropils, usually innervated by lateral-tract neurons. This neuron rather seemed to enfold a region positioned posteriorly of the AL, possibly the lateral accessory lobe (LAL). Nonetheless, based on the neurite`s point of exit from the AL it was classified as a lALT PN.

3.2.3. Mediolateral antennal lobe tract neurons

Two mlALT neurons were stained, both with cell bodies in the LCC, and multiglomerular dendritic arborizations. The neurons were quite weakly stained. In one mediolateral-tract PN, the lateral protocerebral innervations were barely visible, and identification of innervated neuropils was not possible. The other mlALT PN projected only to the LH.

3.2.4. Transverse antennal lobe tract neurons

Three tALT PNs were stained, two of which are displayed in Figure 12. All tALT neurons were multiglomerular and had somata in the LCC. Their axons exited the AL medially, running posteriorly alongside the mALT, until reaching the posterior side of the central body. At this point, the axons of all tALT PNs split off from the mALT and turned laterally. The neuron displayed in Figure 12 A innervated one glomerulus in the posterior complex heavily and two ordinary glomeruli weakly. From the splitting point from the medial- tract, a thick branch projected antero-laterally, innervating the LH and the AVLP. Then, this branch continued postero-medially, innervating both the lateral and medial calyx. A second, finer sub-branch only innervated the medial calyx. The two branches did not overlap in the medial calyx, however the terminals of both branches innervated proximate regions.

The PN in Figure 12 B had thin dendritic neurites spreading throughout large parts of the AL. As the axon split off from the medial tract, one branch projected to the LH, extending a few projection terminals on its route (i.e. in the SNP). A second branch projected to the dorso-medial SNP. Again, the terminals of the two sub-branches innervated adjacent regions.

The third tALT PN, which was relatively weakly stained, had dendrites in two PCx glomeruli and in the antennal hub. After leaving the medial-tract, one axonal sub-branch of the neuron ran directly to the LH whereas a second turned dorso-laterally, projecting through the SNP on its route to the LH, axon terminals were observed in both these neuropils. The two sub-branches did not overlap in the LH, as the terminals of the first sub-branch were positioned slightly anteriorly to those of the second.

3.2.5. Local interneurons

In comparison to AL PNs, local interneurons (Figure 13) were infrequently stained. In total, four preparations held only LNs (Table 4). All LNs were multiglomerular and primarily had dendrites in ordinary glomeruli. One LN had asymmetrical dendrites, with densely distributed dendrites in two glomeruli, one of which was the LPOG, and several sparse dendrites in other glomeruli. This preparation held several stained somata, only the LN displayed in appendix Figure C2 was strongly stained. The other three LNs had only sparse glomerular innervations, and mostly thin neurites. Two of the LNs appeared to have oligoglomerular dendrites, innervating glomeruli only in restricted regions.

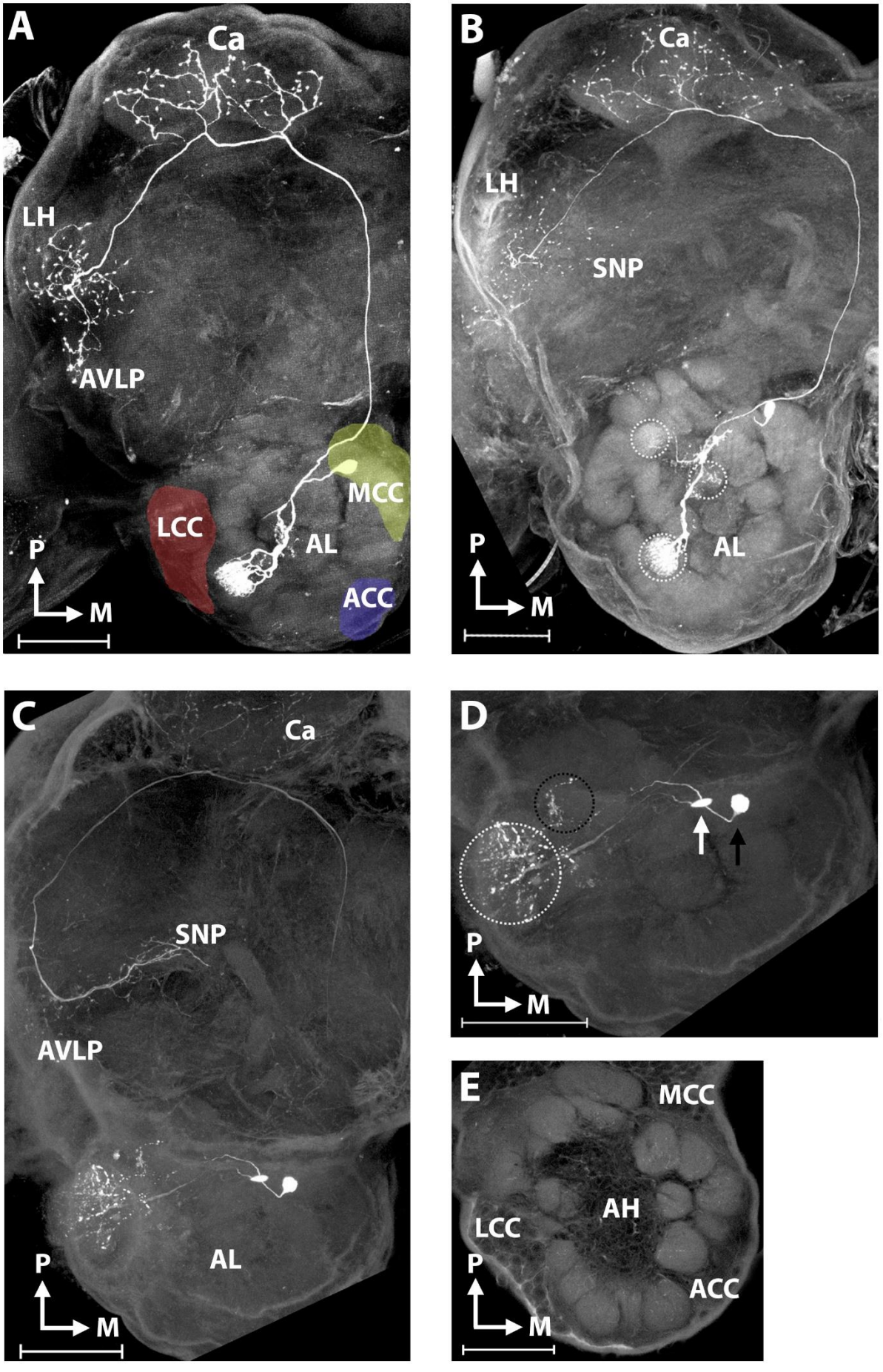
A
Ca
LH
AVLP
MCC
LCC
AL
ACC
P
M
B
Ca
LH
SNP
AL
P
M
C
Ca
SNP
AVLP
AL
P
M
D
P
M
E
MCC
AH
LCC
ACC
P
M

Figure 9. Confocal images in dorsal view. **A)** An uniglomerular medial antennal lobe tract (mALT) projection neuron (PN) (ID: 26/12 m1), which also sent neurites into the antennal lobe hub. The soma was in the medial cell body cluster (MCC), projections went to the calyces (Ca), the lateral horn (LH) and the anterior ventro-lateral protocerebrum (AVLP). Lateral (LCC; in red), anterior (ACC; in blue) and medial (MCC; yellow) cell body clusters in the antennal lobe (AL) are marked. **B)** A multiglomerular (white dotted circles) mALT PN (ID: 4/1 m2). The soma was in the MCC, projections found in the calyces, LH and the superior neuropil (SNP). **C-D)** Two mALT PNs (ID: 8/12 m4), one innervating the cumulus of the macroglomerular complex (white arrow and dotted circle in **D** indicates soma and dendritic arborizations, respectively). The other PN innervated a posterior complex glomerulus (black arrow and dotted circle). Somata were in the MCC, and innervations were seen in the calyces and AVLP. In the protocerebrum, the two axons were untraceable. **E)** An image displaying a ventral position in the AL. Here, the cell body clusters and the antennal lobe hub (AH) are marked. Scale bars: 100 µm.

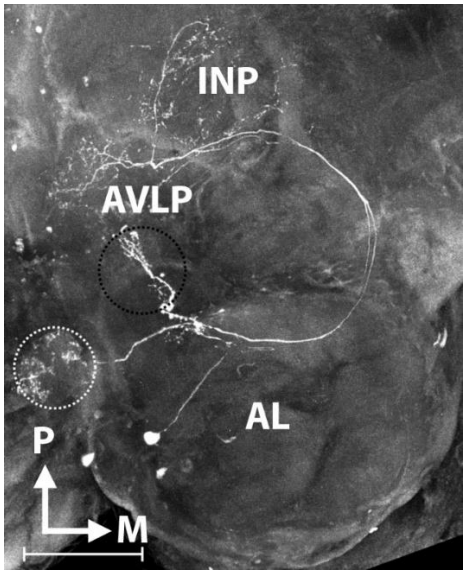

Figure 10. Two lateral-tract neurons (ID: 28/11 m2), in dorsal view. One had dendrites in the cumulus (white dotted circle) and the other in a posterior complex (PCx) glomerulus (black dotted circle). The lateral side of the antennal lobe (AL) was distorted during dissection. Somata were in the lateral cell cluster, projections were in the anterior ventro-lateral protocerebrum (AVLP) and the inferior neuropil (INP). Scale bar: 100 µm.

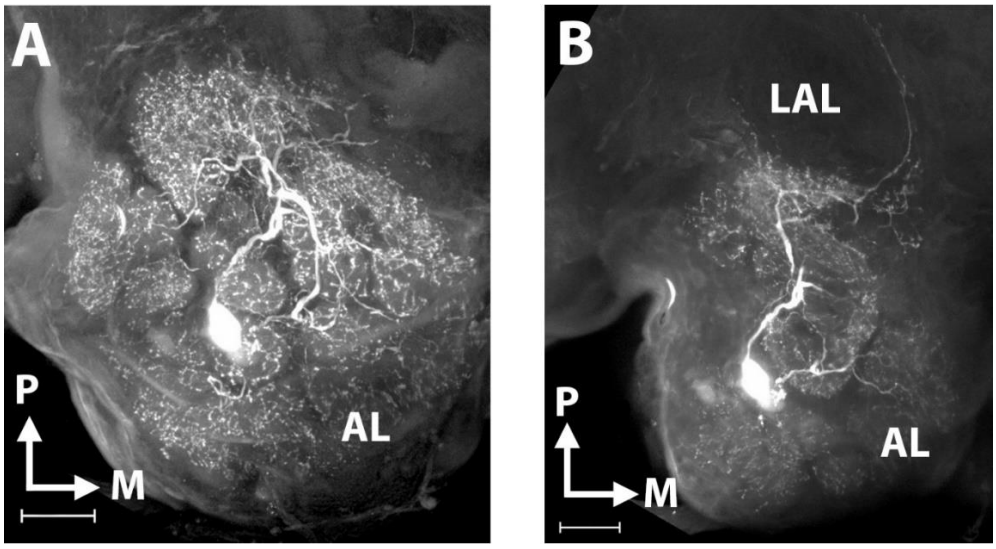

Figure 11. An atypical antennal lobe (AL) neuron, defined as a lateral antennal lobe tract projection neuron (ID: 18/1 m5), in dorsal view. **A)** This neuron was panglomerular, the soma was in the lateral cell cluster. The most posterior neurites extended slightly outside the AL. **B)** An image of the same neuron as in **A**, but covering a more ventral region. Here, neurites projecting posteriorly into the protocerebrum are seen, they appeared to encompass the lateral accessory lobes (LAL). Scale bars: 50 µm.

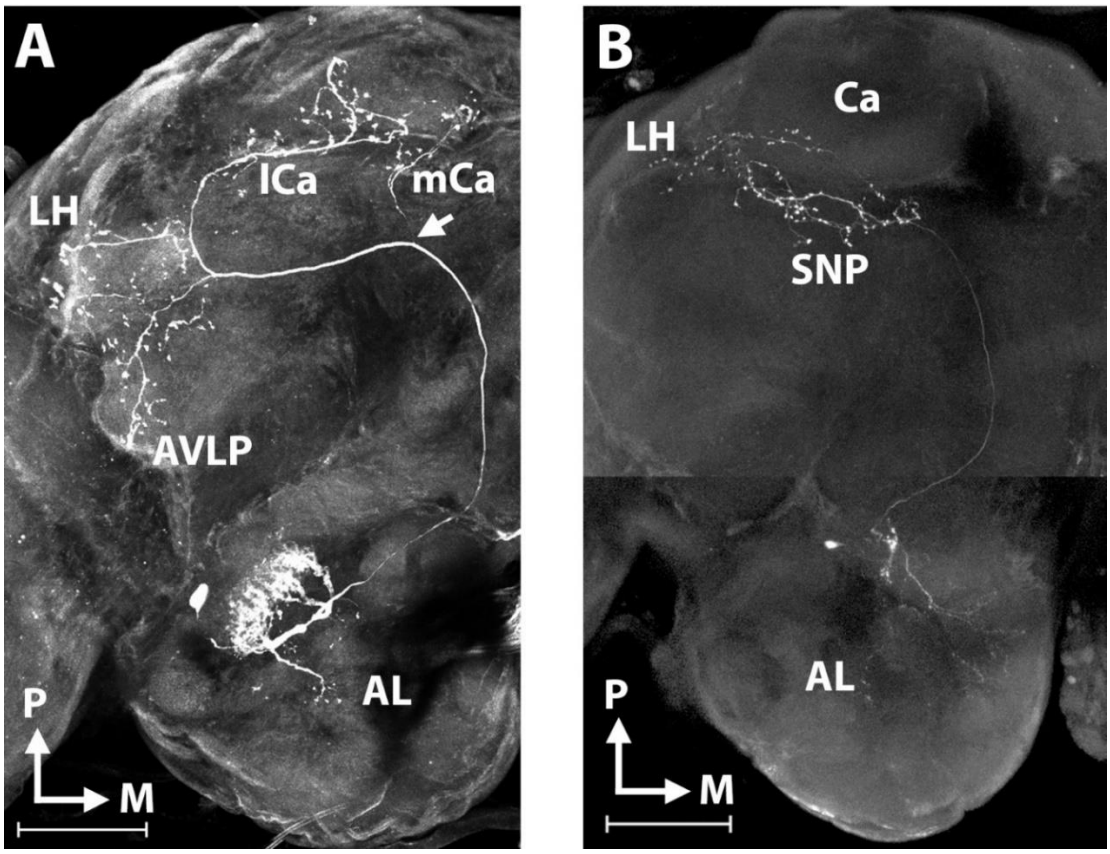

Figure 12. Confocal images of transverse antennal lobe tract (tALT) projection neurons (PNs), in dorsal view. **A)** A multiglomerular tALT PN (ID: 9/12 m6), with the soma located in the lateral cell body cluster (LCC) of the antennal lobe (AL). Two branches innervated the medial calyx (mCa). The main branch also innervated the lateral horn (LH), the anterior ventro-lateral protocerebrum (AVLP), and the lateral calyx (lCa). The short white arrow points to the site where the thin sub-branch left the main branch. **B)** Two images, merged to show another multiglomerular tALT PN (ID: 7/1 m1). The soma was located in the LCC. One sub-branch innervated the LH and the superior neuropil (SNP) while a second sub-branch innervated only the SNP. Scale bars: 100 μm.

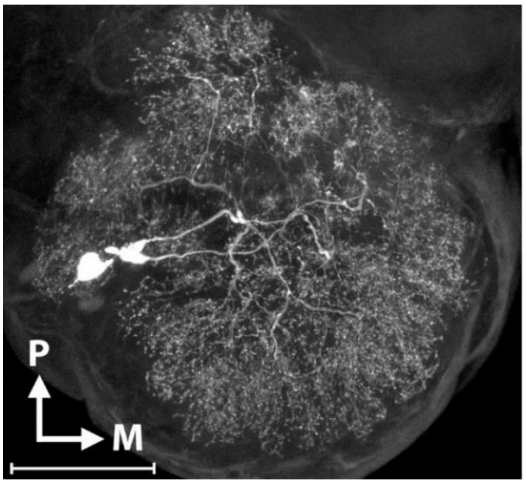

Figure 13. Confocal image of three simultaneously stained local interneurons (ID: 210217M2), confined to the antennal lobe, in dorsal view. Somata were in the lateral cell body cluster, and dendritic innervations were in all glomeruli, including those of the macroglomerular complex. Neuron provided by Xi Chu. Scale bar: 100 μm.

Table 3

Overview of iontophoretically stained projection neurons.

ID	Cell body	Dendritic arborizations	Terminal projections	Statistical analysis	Figure	Notes
mALT						
7/12 m2	LCC	MG	NC	Incl.		Twisted
8/12 m2	LCC	MG	Ca; LH	Incl.		
8/12 m4	MCC	UG Cu; PCx	Ca; AVLP; SNP	Incl.*	9C, D	2 PNs
9/12 m1	NC	MG	Ca; LH	Incl.		
9/12 m5	NC	UG	Ca; LH	Incl.		
11/12 m1	LCC	MG	Ca	Incl.		LH NS
15/12 m1	MCC	UG Cu	Ca; LH; AVLP; SNP	Incl.*		2 PNs
26/12 m1	MCC	UG	Ca; LH; AVLP	Incl.	9A	
26/12 m5	LCC	UG	Ca; LH; AVLP; INP	Incl.	C1A	
28/12 m3	NC	UG MGC	Ca; LH; AVLP	Incl.*	C1C, D	3 PNs
29/12 m1	MCC	UG Cu; OG	Ca, LH, AVLP, INP	Incl.*		2 PNs
29/12 m2	NC	UG PCx	Ca; LH; AVLP	Incl.*		2 PNs
9/1 m3	ACC	UG	Ca; LH; AVLP	Incl.	C1B	
4/1 m2	MCC	MG PCx, OG	Ca; LH; SNP	Excl.	9B	
lALT						
4/1 m3	NC	NC	IL LH; IL AVLP; CL.P	Incl.		WS
9/1 m2	LCC	MG	AVLP; VMNP	Incl.*		3 PNs
28/11 m2	LCC	UG Cu; PCx	AVLP; INP	Excl.	10	2 PNs
29/11 m2	LCC	OG	INP; AVLP; LH	Excl.		
18/1 m5	LCC	MG	Enfolding LAL	Excl.	11A, B	
mlALT						
9/12 m3	LCC	MG	LH	Incl.		
28/12 m2	LCC	MG	Lateral Protocerebrum	Incl.		WS
tALT						
8/12 m3	LCC	MG PCx	Base of Ca; LH	Incl.		WS
9/12 m6	LCC	MG PCx, OG	LH; AVLP; Ca	Incl.	12A	
7/1 m1	LCC	MG	LH; SNP	Incl.	12B	

Note: *= Statistically analyzed as one neuron.
Unless otherwise noted, dendritic arborizations were in ordinary glomeruli or indistinguishable.
Abbreviations: ACC - anterior cell cluster; AVLP – anterior ventro-lateral protocerebrum; C1 – appendix C Figure 1; Ca - calyces of the mushroom bodies; CL.P - contralateral projection; Cu – cumulus of the macroglomerular complex; IL - ipsilateral; INP - inferior neuropil; LAL – lateral accessory lobe; LCC - lateral cell cluster; LH - lateral horn; MCC - medial cell cluster; MG - multiglomerular; MGC – macroglomerular complex; NC - not conclusive; NS – not seen; OG - ordinary glomeruli; PCx - posterior complex; PN – projection neuron; SNP - superior neuropil; UG - uniglomerular; VMNP - ventro-medial neuropil; WS – weakly stained.

Table 4

Local interneurons morphology

ID	Cell body	Dendritic arborizations	Stat. Analy.	Figure	Notes
23/11 m1	LCC	Multiglomerular Sparse OGs	Excl.		WS
29/11 m1	LCC	Multiglomerular OlG Sparse OGs	Incl.		WS
6/12 m2	LCC	Multiglomerular OlG Sparse OGs	Incl.		WS
4/1 m1	LCC	Multiglomerular AS OGs, LPOG	Incl.*	C2	Several LNs

Note: * = Statistically analyzed as one neuron.
Abbreviations: AS – asymmetric; C2 – appendix Figure C2; LCC – lateral cell body cluster; LN – local interneuron; LPOG – labial-palp pit organ glomerulus; OG – ordinary glomeruli; OlG – oligoglomerular; WS – weakly stained.

4. Discussion

In this thesis, identification into neuron categories based on electrophysiological parameters was achieved. A significant categorization of LNs and PNs correctly classified 76% of the sampled neurons using three physiological parameters. There were, however, no significant differences between the two neuron categories on any individual physiological parameter.

For projection neurons, a cluster analysis found two sub-categories based on electrophysiological parameters. These clusters did not significantly correspond with the tract or glomerular innervation of the PNs. Novel findings were presented on physiological differences between structurally separate PN categories. Spike duration was significantly higher in the mALT than in the remaining tracts pooled, and the spontaneous firing rate was significantly higher in uniglomerular PNs than in multiglomerular PNs.

Additionally, 24 PNs and four LNs were morphologically described. Three of these PNs were tALT neurons. Only one individually stained neuron has previously been classified as a tALT PN in *Heliothine* moths (Ian et al., 2016b). Previous findings of divergent termination patterns for MGC and OG medial-tract neurons were also supported by findings presented here.

4.1. Local interneuron and projection neuron electrophysiology

4.1.1. Cluster analyses

We initially ran a cluster analysis with all six physiological parameters, i.e. ISI mean, ISI cV, spontaneous firing rate, FF, spike duration and FWHM, then reran the analysis with only the spontaneous firing rate, FF and spike duration. The classification performance was indistinguishable for these two analyses, indicating that the inclusion of all six parameters offered no benefits. The ISI cV and spontaneous firing rate had a strong positive correlation (r (46) = .61, $p < .001$), as did FWHM and spike duration (r (46) = .98, $p < .001$), which establishes a lack of independence in the first cluster analysis. With previous reports indicating that FF $\propto$ = cV^2 $\propto$ (Nawrot et al., 2008), it was surprising to find that ISI cV and FF were not significantly correlated (r (46) = .03, p = .86), nor was ISI cV^2 and FF (r (46) = .23, p = .12). The second analysis allowed for independence of the variables included, as none of the three entered parameters were significantly correlated ($r > .08$). In addition, the inclusion of only three parameters offers for a parsimonious model. In comparison, the models reported by Lei et al. (2011) and Meyer et al. (2013) required nine and five parameters, respectively, yet the last mentioned study reduced their five parameters to three

principal components (explaining 75% variance), which were used in their final cluster analysis. Their models, however, had higher classification-abilities than that presented here, as both boasted 90% correct classification.

Our results were dependent on the clustering method. When using Euclidian distances instead of Log likelihood as a distance measure, the cluster analysis converged on one cluster, rather than two. Additionally, several of the parameters used in Lei et al. (2011) could have been beneficial to include in our model, such as parameters detecting burstiness, or quantifying burst duration and number of spikes within bursts. Other parameters, we refrained from using due to their limitations. For example, spike amplitude was initially calculated, but we chose to omit this from the statistical analyses due to differences in amplitude as a function of recording location along a somatodendritic axis (Harris, Henze, Csicsvari, Hirase, & Buzsáki, 2000). This implies that any systematic variation in distances between somata and recording location could have skewed values in a neuron category-dependent manner for the amplitude.

Our motivation for investigating the possibility of classifying neuron category prior to staining was quite simple, and had clear potential benefits to future intracellular recording in the insect AL: As the intracellular recording technique is used, the researcher has no way of identifying neuron category prior to iontophoretic staining. In mapping the olfactory pathways, the hypotheses tested will regularly be related to certain neuron types. As such, an ability to estimate neuron category while recording could decrease the chances of staining unsolicited neurons, and estimation of neuron category could be accomplished for incomplete stains. Furthermore, neuron labelling would not necessarily be required. Neuron category estimation used instead of staining has been attempted in moths previously, Christensen et al. (1993) relied singularly on physiological criteria to classify neuron categories in *M. sexta* while using multiple recording electrodes to investigate LN-PN interactions. In that study, no staining was applied, reportedly due to an increase of noise when using dye-filled microelectrodes. Some of the physiological parameters used by Christensen et al. (1993) were related to responses to odor stimulation. In this thesis, the focal point was rather the spontaneous activity of AL neurons.

Ideally, we would have used a machine learning approach, which could have been used to build a model by an iterative and automatic process. This approach revolves around finding an optimal solution for classification based on a set of parameters, using only a limited part of the total sample. The resulting model could then be used to predict neuron category for a test sample, to evaluate the performance of the model (Mohri, Rostamizadeh, &

Talwalkar, 2012). A highly efficient model could later be applied to new data, possibly allowing for neuron categorization with or without staining. Such an approach was taken by Lei et al. (2011), as they used the moth *M. sexta* to classify neuron category through an iterative (1000 repeats) classification algorithm. They used nine parameters quantifying the burstiness in spontaneous spiking activity, in addition they added neuron category into their analysis. Through this procedure, they found an average of 80% correct classification of morphological category, with 90% being their maximum accuracy. In contrast, we only assessed burstiness through the ISI cV, for which high values does not necessarily associate with burstiness (see section 1.1.1.). This parameter was also removed from the final model, without affecting the model`s classification performance.

While we found classification based on physiological parameters in *H. armigera* to have a significant goodness-of-fit with morphological classification of LNs and PNs, 24% of the sampled neurons were misclassified. In comparison, on average 20% of LNs and PNs were misclassified in *M. sexta* (Lei et al., 2011). This level of error should invoke caution in the interpretation of the classifying ability of the used parameters. It would seem inappropriate to classify neuron category solely based on physiology, in absence of any morphological data.

4.1.2. Equality of spontaneous spiking patterns between neuron categories

Another finding indicating the inadequacy of classification based exclusively on the physiological parameters used, is the lack of significant group differences between LNs and PNs in any of the six physiological parameters. As seen in Table 4, the spread around the means of all physiological parameters was rather large, as demonstrated by high standard deviations. This was particularly the case for the LNs, where the standard deviations were substantially higher than what was observed for the PNs. One of the reasons for this high spread, could be that the sample size for the LNs was much lower than for the PNs, with only 10 LNs compared to 36 PNs. In comparison, the study reported by Lei et al. (2011) included 85 LNs and 63 PNs. With this spread, followed substantial overlap of parameter values for the LNs and PNs, however this was also reported for the ISI cV by Lei et al. (2011). In a small sample, any outliers, or extreme parameter values, will increase the within-group variance considerably, obscuring potential statistical effects. It was assumed that all parameter values for individual neurons was representative of randomly sampled variance belonging to the targeted neuron populations. Furthermore, a basic assumption in dealing with outliers is that these extreme values could originate from cases not sampled from the same population as

other sampled cases (e.g. Dixon, 1953). This assumption should not apply here. The sampled neurons were already validated as belonging either to LN or PN populations through morphological classification, although such classification might have been imperfect. The effects of outliers were also likely mitigated by means of using the *Mann-Whitney U-test*, which compares the sums of ranked data between groups (Fay & Proschan, 2010).

4.1.2.1. Interspike intervals and spontaneous firing rate

We found no significant differences between LNs and PNs on any of the ISI parameters, i.e. ISI mean and ISI cV, nor for the related parameters spontaneous firing rate and FF. Contrarily, Lei et al. (2011) found PNs to be more bursty than LNs, one of the parameters signifying this was high values of ISI cV for the PNs. Their finding seems coherent to the functions of these neuron categories, in regard to odor responses. Burstiness is associated with reliability in terms of transmitting information to postsynaptic neurons (reviewed by Lisman, 1997), thus bursty PNs should be well equipped for conveying odor information to third order odor neurons. Indeed, for *M. sexta* it was reported that for bursty MGC PNs, there was a strong positive correlation between spontaneous burstiness and firing rate during odor stimulation, as well as spontaneous burstiness and spontaneous firing rate. This demonstrated that PNs with bursty spontaneous spiking patterns would strongly innervate output regions in the protocerebrum when stimulated with odorants. LNs, on the other hand, serve AL modulatory functions through release of primarily the inhibitory neurotransmitter GABA. Panglomerular LNs, as seen in Figure 13, could serve to globally inhibit the AL through tonic, regular firing patterns. Silbering and Galizia (2007) suggests that such global inhibition could suppress odor responsiveness in all glomeruli. Meanwhile, excitatory input from OSNs (Sanes & Hildebrand, 1976) and excitatory LNs (Chou et al., 2010; Shang et al., 2007) could augment responsiveness in PNs of specific glomeruli, thus providing gain control. In our sample, however, the pooled ISI distributions of PN and LN categories, plotted in Figure 8, indicated no major differences in spontaneous firing patterns, and a large degree of variance overlap. Indeed, the differences in ISI distributions were not significant, as tested by the *mixed ANOVA*.

While there is of course the possibility of burstiness being different in *M. sexta* and *H. armigera*, it seems likely that spontaneous and odor response spiking activity may be similar in these related species. Our failure in replicating differences in ISI irregularity may be explained in part by our low LN sample, and in part by sampling deficiencies. An inattentiveness to a morphological feature that may be crucial to the recording of

physiological activity in LNs, could have caused the low LN sample. The neurites of the LNs are quite thin in most regions other than the antennal lobe hub, this region is therefore the most likely place to achieve good neuron contact, given a reported bias towards contacting thick neurites (Seki & Kanzaki, 2008). Rather than aiming for the antennal lobe hub, microelectrodes were often aimed at postero-lateral regions of the AL, which holds neurites of MGC neurons. Such neurons were sampled as they could prove useful in future analyses at our lab. Moreover, Seki et al. (2010) point out that LNs could operate with global and local properties. Dendritic EPSPs would constitute local properties, while action potentials from the thick main neurite would be a global property (Christensen et al., 2001). As such, recorded physiology may be a result of recording location. Recording from the glomeruli in the postero-lateral AL may have caused the recording of both local and global properties, biasing the ISI, firing rate and waveform parameter values for the sampled LNs.

Additionally, several of the sampled LNs were quite weakly stained. This was likely a result of poor neuron contact in the glomeruli, where LNs regularly had sparse dendritic innervations. This could have led to incomplete neuron labelling, which may have caused morphological misclassification. Some of the most recently sampled LNs, such as that displayed in Figure 13, were sampled by inserting the microelectrode into the antennal lobe hub, these stains appeared to provide complete neuron labelling.

4.1.2.2. Waveform parameters.

Also for the waveform parameters, i.e. the FWHM and spike duration, there were no significant differences between the LNs and PNs. This was unanticipated, as the FWHM has been reported to be almost twice as large in LNs (2.3 ms ± 0.2 ms) as in PNs (1.2. ms ± 0.1. ms) in *M. sexta* (Christensen et al., 1993). Furthermore, longer spike duration is associated with higher neurotransmitter release through lengthy exocytosis (Deng et al., 2013; Hochner et al., 1986), which should suit the main function of GABAergic LNs, i.e. downregulating activity across the antennal lobe. However, all sampling limitations discussed in section 4.1.2.1. may also apply here, these could have biased our results, resulting in non-replication of the findings reported by Christensen et al. (1993). Yet, a recent study on another moth species, *Bombyx mori,* also reported on FWHM in LNs (1.98 ms ± 0.1 ms) and PNs (1.96 ms ± 0.06 ms), however there were no apparent differences in this parameter (Tabuchi et al., 2015). The findings of (Christensen et al., 1993) may thus be species-specific, or a result of skewed sampling, given the small sample size.

4.2. Projection neuron physiology

4.2.1. Cluster analyses

In performing a cluster analysis to investigate sub-categories of PN, which has not previously been done for insects, we used all six spontaneous spiking parameters (see Table 1) and three parameters: the spontaneous firing rate, FF and spike duration. The results were identical, implying that the addition of ISI mean, ISI cV and FWHM offered no more than undesirable dependence among variables, only the analysis with three parameters was therefore reported. The cluster analysis converged on two clusters. We found that these clusters did not significantly align with PNs in different tracts, which were defined as mALT PNs and other ALTs PNs (ml-, l- and tALT pooled together). In the honeybee, differences in physiological properties has been reported for medial and lateral tracts, however these differences were related to odor response-range, not spontaneous activity (Brill et al., 2013). To our knowledge, no reported findings on electrophysiological differences of spontaneous activity in the separate ALTs are available.

The motivation to investigate differences between the ALTs, was that the mALT has been found to be dominated by uniglomerular PNs, while the ml- and lALT has been found to possess a comparatively higher ratio of multiglomerular PNs (Homberg et al., 1988; Ian et al., 2016b). Any such assumptions regarding the tALT would be precipitant, as the transverse tract has not yet been sufficiently charted. However, all reported singularly stained tALT PNs in *Heliothine* moths (including the three reported in section 3.2.4.) innervated multiple glomeruli (Ian et al., 2016b), consistent with findings for *Drosophila* tALT PNs (Tanaka, Endo, & Ito, 2012). These structural differences between the tracts could be anticipated to be associated with functional differences in electrophysiological properties. Tract discrimination did not fully separate uni- and multiglomerular PNs. Accordingly, matching the found clusters to observed dendritic arborizations seemed pertinent to test the hypothesis that dendritic structure within the AL could be associated with physiological differences. However, there was no significant fit with dendritic arborizations, which was defined as uniglomerular or multiglomerular. In consequence, there seems to be no validity in classifying PN ALT or whether PNs were uni- or multiglomerular based on the electrophysiological parameters used in our cluster analyses.

Lei et al. (2011) reported significant differences for two categories of PNs, i.e. MGC PNs and ordinary PNs, on the parameter local variation (Lv). This parameter is related to the ISI cV, yet it is more robust to non-stationarity (see section 4.3.3. for discussion of non-stationarity). Due to these reports, we hypothesized that the presence of two separate PN

clusters could be coherent with functionally separate olfactory sub-systems, however we lacked the MGC sample size necessitated to investigate this matter.

4.2.2. Physiological differences between projection neuron categories

Here, we reported novel findings on physiological differences between morphologically distinct PN categories. There were significant differences in spike duration between the PNs in the medial-tract and the other ALTs. Specifically, the mALT displayed longer spike duration than the other tracts pooled. As previously mentioned, differences in spike duration can have implications for the influx of Ca^{2+} into the presynaptic terminals, thus affecting the duration of exocytosis. As such, for the primarily cholinergic PNs (Bicker, 1999; Yasuyama et al., 2002) of the mALT, individual spikes could lead to release of higher amounts of neurotransmitter than single spikes in other tracts.

Additionally, the uniglomerular PNs had a significantly higher spontaneous firing rate than multiglomerular PNs. It appears that thicker axons diameters are more easily excitable than thinner axons (reviewed by Koester & Siegelbaum, 2013b). We were under the impression that the uniglomerular PNs, particularly those of the mALT, had comparatively thicker axons than that of the multiglomerular PNs, this could imply that the higher spontaneous firing rate was a physical property of the neurons, rather than specifically related to odor processing. To test this hypothesis, we randomly shuffled our data-set, and measured the axon diameter at the exit point from the AL for five uniglomerular and five multiglomerular PNs using the ZEN software. We found no statistical difference for uniglomerular (M = 2.80 μm, SD = 0.85 μm) and multiglomerular (M = 2.26 μm, SD = 0.71 μm) PNs, yet this requires a considerably more thorough investigation, and a larger tested sample-size, to offer any conclusions.

The ISI distributions separated by ALT partition or glomerular arborizations were not different. However, there appears to be a trend where the ISI cV is high for uniglomerular PNs (see Figure 8 B; Table 4). In Lei et al. (2011), they reported higher ISI cV for PNs than LNs, but there were no reports of the amount of PNs that were uni- or multiglomerular. They do, however, describe PNs as primarily uniglomerular. This could offer an explanation to why they found significant differences in LN and PN ISI cV, which were not replicated in this thesis.

4.3. Methodological considerations and limitations

4.3.1. Sampling strategies

Our sample for statistical analysis consisted of 10 LNs and 36 PNs, the LN sample was quite low. Low sample-sizes yields low statistical power, which can increase the probabilities of introducing both type I and type II errors (false positive and false negative, respectively), (reviewed by Button et al., 2013). The limited sample size of LNs was likely to have been partially caused by the PNs greatly outnumbering the LNs, as the count of LNs and PNs in the related species *M. sexta* has been reported to be approximately 360 LNs and 850 PNs (Homberg et al., 1988). Additionally, none of the stained LNs demonstrated any clear odor responses. During intracellular recording, if the contacted neuron was not perceived as odor responsive, it was ordinarily not stained. A calcium imaging study found odor response strength to be higher in PNs than in LNs (Silbering, Okada, Ito, & Galizia, 2008). As PNs may be expected to display clearer responses to stimulation, a bias towards PN staining may have been introduced. As mentioned in section 4.1.2.1., the microelectrodes were also inserted in postero-medial regions, rather than in the antennal lobe hub, which would have been optimal for LN sampling. On some occasions, simply permeating the antennal lobe itself proved a challenge, making exact regional discrimination unachievable. Some moths would produce considerable amounts of extracellular fluid, upon which a sheath formed. This sheath covered the brain and impeded visibility. The staining of a visual neuron, displayed in appendix Figure A1 C, serves as testament to such challenges.

4.3.2. Intracellular recording and noise

In the initial stages of data gathering, the microelectrodes frequently broke, leading to dye-leakages that could leave the preparation inapplicable to morphological classification. A new filament had been introduced to the microelectrode puller, and appropriate adjustments of puller settings had not been performed. A ramp-test was executed to identify suitable heat settings for the microelectrode puller (P-97 Flaming-Brown™ Micropipette Puller Operation Manual, 2016), temperatures at 298 ± 25 °C were found to be optimal. We then performed experiments with more than a dozen different puller-settings. After assessing resistance, perceived ease in establishing neuron contact, and stain-quality, a satisfactory puller-setting was found (heat - 315; pull – 80; velocity – 70; time - 250). Post-staining resistances were then in the range of 70-350 MΩ. A lower resistance could indicate microelectrode breakage, which led to electrode replacement. Conversely, if the resistance was too high, sometimes up to 1000 MΩ, the microelectrode could be overly sensitive to minor voltage fluctuations.

In the process of spike analysis, spike sorting was crucial in dealing with recorded noise. Eight neurons had to be excluded from statistical analyses due to difficulties in finding wavemarks which fit the waveforms recorded. This was normally due to inclusion of noise, which prohibited efficient separation of the action potential signal and seemingly inconsequential voltage fluctuations. Failure in creating suitable wavemarks could result in noise being counted as events (which should represent action potentials), and action potentials failing to be considered as events, necessitating exclusion from the statistical analyses.

4.3.3. Spike train analyses

When processing spike train data, the observed spike trains are assumed to be stochastic point processes. Spike trains are *stochastic* by being representative of randomly sampled activity, and *point processes* by containing indistinguishable individual spikes (Moore et al., 1966). In attempting to ensure that the analyzed spike trains were point processes, differing wavemarks would be merged only when their spike durations and shapes were comparable. Differences in neuron contact due to microelectrode drift, activity-dependent waveform change (e.g. during bursts) or multiple contacted neurons could cause waveform variability (Fee, Mitra, & Kleinfeld, 1996). Multiple wavemarks were additionally only merged if confocal data gave unambiguous reason to assume these originated from homogeneous neurons. Moreover, spike sorting would ordinarily allow for exclusion of minor membrane fluctuations, potentially from additional neurons. The sampled activity was assumed to be stochastic through the random variations in the interspike interval (Moore et al., 1966), which required the absence of influences leading to systematic variation.

Another central assumption is that of stationarity, which implies that the sample of spikes processed are not dependent on the time from which the sample was drawn (Moore et al., 1966). Conversely, non-stationarity signifies that the distribution of the observed spike train is contingent upon the time of sampling, such effects can be introduced by stimulation (Nawrot, 2010; Perkel et al., 1967). This suggests that spontaneous activity is ideally analyzed in recordings void of stimulation. The collection of stimulation data was yet considered beneficial, as such data can prove applicable to subsequent analyses at our lab. As little stimulation-free recordings were available, the spontaneous activity was sampled from the pre-stimulation windows. This is the data generally used to estimate spontaneous activity when analyzing response characteristics (e.g. Meyer et al., 2013; Reisenman et al., 2011). To manage our concerns regarding non-stationarity, stimulations less than five seconds apart were deleted. Also, a second trial with any stimulus would not be applied until the

experimenter perceived the neuron to have retained its spontaneous firing pattern. The presence of stimulation in the data still upholds the possibility that non-stationary effects could exist in some of the analyzed data.

For the ISI cV and the FF, longer observation times leads to more accurate estimates of population values (Nawrot, 2010). The estimates of the FF are optimal when the expected spike count in a certain observation window exceeds 10, while ISI cV requires 5-10 expected spikes, this applies to Poisson processes (Nawrot et al., 2008). More regular processes reach optimal estimates faster, while more irregular processes necessitate higher expected count of spikes. Here, the spontaneous firing rate serves as an estimate of expected spike count for each observation window. With Poisson processes having an ISI cV = 1 (van Vreeswijk, 2010), the spontaneous firing rate could be too low for optimal FF estimates for two neurons in our data (ID: 141016M2; 171116M1), while it is below the requirements for good estimates of both the ISI cV and the FF for another two neurons (ID: 9/12 m3; 9/12 m6; see appendix Table E1 for parameter values). No neurons were however excluded on these grounds.

4.3.4. On statistical inference and study design

As the number of related statistical tests performed using the same data expand, the probability of introducing type I errors (false positives) increase exponentially. This is known as the familywise error rate, with family referring to a "family" of tested hypotheses. What constitutes such a family is up for discussion, a data-set used for different purposes could be regarded as separate families (reviewed by Shaffer, 1995). For exploratory studies, it is not uncommon that numerous related hypotheses are statistically tested. This practice has nonetheless received substantial amounts of criticism, due to the increased probability of type I errors in exploratory designs (e.g. Ioannidis, 2005). Studies with exploratory designs, such as this thesis, should be interpreted with caution when making inferences to target populations. For this to be appropriate, *p*-level adjustments ought to be applied to control for the familywise error rate, for example with the conservative (Frane, 2015) and commonly used Bonferroni adjustment (e.g. in Zhemchuzhnikov, Kutcherov, Kymre, & Knyazev, 2017). Such corrections were not applied in this thesis. Nevertheless, the statistical results presented in this thesis were not intended to stand on their own, but rather to inform future confirmatory studies, with fewer tested hypotheses.

4.4. Morphological findings

The neuroanatomy of the neurons gathered was considered secondary to the statistical analyses of neuron category physiological characteristics, however, several interesting morphological findings were presented in this thesis[2]. Among these, were novel findings made on the transverse-tract, with three tALT PNs labelled. Ian et al. (2016a) first reported on this tract in *Lepidoptera* after locating it in mass stains, subsequently Ian et al. (2016b) presented one individually stained tALT PN. Tanaka et al. (2012) had previously presented four sub-categories of the tALT in *Drosophila*, and compared it to three heterogeneous categories of mediolateral ALTs in *Hymenopteran* species, such as *A. mellifera*. Correspondingly, the previously described *Heliothine* tALT PN and the three reported in this thesis, show a large degree of heterogeneity. Due to resemblances with the mlALT, it may be that tALT PNs have been reported as mlALT PNs in some of the previous studies on olfactory pathways in *Heliothine* species (e.g. Type 2 ml-APT in Løfaldli et al., 2012). The three transverse-tract neurons reported here had dissimilar innervation patterns in the protocerebrum, as each of these neurons innervated different protocerebral neuropils with two distinct branches (see section 3.2.4.).

One neuron, classified as a lALT PN (ID: 18/1 m5, see Figure 11) was particularly hard to classify. This neuron was initially classified as a LN due to the absence of axonal innervations of lateral protocerebral neuropils such as the AVLP or LH, however thin neurites did extend beyond the AL. The neurites seemed to enfold the lateral accessory lobe (LAL). This necessitated classification as a PN, as LNs should be confined to the AL. The neuron was classified as belonging to the lateral tract. Due to uncertainties regarding the neuron`s classification, this neuron was omitted from the statistical analyses. However, re-running the cluster analysis (using the spontaneous firing rate, FF, and spike duration) with this neuron included in the analysis, demonstrated that the physiological properties of this neuron was more similar to LNs than PNs. This neuron, assumed to be a lateral-tract neuron, was grouped in cluster 1, where 60% of the LNs were grouped in the previously reported cluster analysis.

The protocerebral innervation patterns of mALT PNs with dendrites in the MGC or ordinary glomeruli (OG) were found to be divergent. In the calyces, the MGC neurons were found to innervate particularly inner regions of the calyces, where innervations were quite sparse (see Figure 9 C; appendix Figure C1 C). The OG neurons innervated larger regions,

[2] On the discussion of morphology, only preparations containing one or at most three homogeneous labelled neurons, are considered. The labelled neurons of any individual preparation are for all purposes described as one neuron, unless otherwise noted.

and had a denser innervation pattern. These findings are corroborative of MGC and OG separations presented by Zhao et al. (2014). It has been shown that for male moths, associations of a plant odor and sucrose reward could be learned, while associating the intraspecific pheromone blend with sucrose failed (Hartlieb, Anderson, & Hansson, 1999). These behavioral findings appear to be coherent with the structural findings on MGC and OG innervations in the calyces. Learning an association between plant odorants (processed by OG PNs) and reward should necessitate a higher extent of processing in the associative odor memory-linked calyces (e.g. De Belle & Heisenberg, 1994) than that of pheromones (processed in the MGC), which has been shown to elicit behavioral responses without associative learning in male moths (e.g. Kehat & Dunkelblum, 1990).

4.4.1. On morphological analysis of projection terminals

The lateral protocerebral neuropils are in many cases indistinct and unclearly delineated from adjacent neuropils, in contrast to for instance the mushroom bodies or the antennal lobes (Ito et al., 2014). Numerous studies have previously reported on olfactory PN terminations in the protocerebrum (e.g. Homberg et al., 1988; Kanzaki et al., 1989; Løfaldli et al., 2012; Rø et al., 2007; Tanaka et al., 2012), but the nomenclature for many protocerebral neuropils has been divergent. For these reasons, the exact areas innervated by the ALTs has been less than clear. In recent years, several developments in insect morphological research has enabled precise "navigation" of the insect brain. An article by a large group of leading insect researchers (Ito et al., 2014) provided a comprehensible morphological description and a uniform nomenclature for the brains of most insect model organisms. Furthermore, databases containing a variety of standardized insect brains has been made available (e.g. Heinze, Pfuhl, & el Jundi, 2015). These enable 3D visualization of neuropils, tracts, and individual neurons gathered through numerous studies. Using the nomenclature from Ito et al. (2014), detailed descriptions of the innervation patterns in the protocerebral neuropils has recently been provided for *Heliothine* moths (e.g. Ian et al., 2016b). Such characterizations, along with those reported in this thesis, have been greatly assisted by these newly available tools.

5. Conclusions

In this thesis, we have demonstrated that statistical classification based on parameters characterizing spontaneous spiking patterns of local interneurons and projection neurons correctly classified 76% of the sampled neurons, in the noctuid moth *Helicoverpa armigera*. This corroborates findings reported in other moth species, and we demonstrated that the classification performance is similar to that reported in *Manduca sexta*, even when using different physiological parameters. Furthermore, we discovered two sub-categories of projection neurons, however we could not identify any morphological feature accounting for this separation, as both ALT partition separating the mALT from the other ALTs, and the separation of uniglomerular and multiglomerular PNs had non-significant fit with the clusters. The differences between PN categories in spike duration and spontaneous firing rate, suggested there may be dissimilarities in release of neurotransmitter for PNs according to tract-allocation and glomerular innervation patterns. Further experiments are required to offer any conclusions on this matter. The statistical findings presented in this thesis can serve to inform future studies investigating physiological properties of distinct AL neuron categories through confirmatory study-designs. Additionally, previous findings demonstrating divergent protocerebral innervation patterns of functionally separate medial tract projection neurons processing pheromone substances and general odorants was conceptually replicated.

References

Akalal, D. B. G., Yu, D., & Davis, R. L. (2010). A late-phase, long-term memory trace forms in the γ neurons of *Drosophila* mushroom bodies after olfactory classical conditioning. *Journal of Neuroscience, 30*(49), 16699-16708. doi:https://doi.org/10.1523/JNEUROSCI

Alving, B. O. (1968). Spontaneous activity in isolated somata of *Aplysia* pacemaker neurons. *The Journal of General Physiology, 51*(1), 29-45. doi:10.1085/jgp.51.1.29

Berg, B. G., Almaas, T. J., Bjaalie, J. G., & Mustaparta, H. (1998). The macroglomerular complex of the antennal lobe in the tobacco budworm moth *Heliothis virescens*: specified subdivision in four compartments according to information about biologically significant compounds. *Journal of comparative Physiology A, 183*(6), 669-682. doi:10.1007/s003590050290

Berg, B. G., Galizia, C. G., Brandt, R., & Mustaparta, H. (2002). Digital atlases of the antennal lobe in two species of tobacco budworm moths, the oriental *Helicoverpa assulta* (male) and the American *Heliothis virescens* (male and female). *Journal of Comparative Neurology, 446*(2), 123-134. doi:10.1002/cne.10180

Berg, B. G., Schachtner, J., & Homberg, U. (2009). γ-Aminobutyric acid immunostaining in the antennal lobe of the moth *Heliothis virescens* and its colocalization with neuropeptides. *Cell and Tissue Research, 335*(3), 593-605. doi:10.1007/s00441-008-0744-z

Bicker, G. (1999). Histochemistry of classical neurotransmitters in antennal lobes and mushroom bodies of the honeybee. *Microscopy research and technique, 45*(3), 174-183. doi:10.1002/(SICI)1097-0029(19990501)45:3<174::AID-JEMT5>3.0.CO;2-U

Brill, M. F., Rosenbaum, T., Reus, I., Kleineidam, C. J., Nawrot, M. P., & Rössler, W. (2013). Parallel processing via a dual olfactory pathway in the honeybee. *Journal of Neuroscience, 33*(6), 2443-2456. doi:https://doi.org/10.1523/JNEUROSCI.4268-12.2013

Button, K. S., Ioannidis, J. P., Mokrysz, C., Nosek, B. A., Flint, J., Robinson, E. S., & Munafò, M. R. (2013). Power failure: why small sample size undermines the reliability of neuroscience. *Nature Reviews Neuroscience, 14*(5), 365-376. doi:10.1038/nrn3475

Chou, Y. H., Spletter, M. L., Yaksi, E., Leong, J. C., Wilson, R. I., & Luo, L. (2010). Diversity and wiring variability of olfactory local interneurons in the *Drosophila* antennal lobe. *Nature neuroscience, 13*(4), 439-449. doi:10.1038/nn.2489

Christensen, T. A., D'Alessandro, G., Lega, J., & Hildebrand, J. G. (2001). Morphometric modeling of olfactory circuits in the insect antennal lobe: I. Simulations of spiking local interneurons. *Biosystems, 61*(2), 143-153. doi:http://doi.org/10.1016/S0303-2647(01)00163-0

Christensen, T. A., Mustaparta, H., & Hildebrand, J. G. (1991). Chemical communication in *Heliothine* moths. *Journal of comparative Physiology A, 169*(3), 259-274. doi:10.1007/BF00206990

Christensen, T. A., Waldrop, B. R., Harrow, I. D., & Hildebrand, J. G. (1993). Local interneurons and information processing in the olfactory glomeruli of the moth *Manduca sexta*. *Journal of comparative Physiology A, 173*(4), 385-399. doi:10.1007/BF00193512

Cohen, J. (1992). A power primer. *Psychological bulletin, 112*(1), 155-159. doi:http://dx.doi.org/10.1037/0033-2909.112.1.155

De Belle, J. S., & Heisenberg, M. (1994). Associative odor learning in *Drosophila* abolished by chemical ablation of mushroom bodies. *Science-AAAS-Weekly Paper Edition-including Guide to Scientific Information, 263*(5147), 692-694. doi:10.1126/science.8303280

Deng, P. Y., Rotman, Z., Blundon, J. A., Cho, Y., Cui, J., Cavalli, V., . . . Klyachko, V. A. (2013). FMRP regulates neurotransmitter release and synaptic information transmission by modulating action potential duration via BK channels. *Neuron, 77*(4), 696-711. doi:http://doi.org/10.1016/j.neuron.2012.12.018

Dixon, W. (1953). Processing data for outliers. *Biometrics, 9*(1), 74-89. doi:10.2307/3001634

Fano, U. (1947). Ionization yield of radiations. II. The fluctuations of the number of ions. *Physical Review, 72*(1), 26-29. doi:https://doi.org/10.1103/PhysRev.72.26

Fay, M. P., & Proschan, M. A. (2010). Wilcoxon-Mann-Whitney or t-test? On assumptions for hypothesis tests and multiple interpretations of decision rules. *Statistics surveys, 4*, 1-39. doi:10.1214/09-SS051

Fee, M. S., Mitra, P. P., & Kleinfeld, D. (1996). Variability of extracellular spike waveforms of cortical neurons. *Journal of Neurophysiology, 76*(6), 3823-3833.

Ferguson, C. J. (2009). An effect size primer: A guide for clinicians and researchers. *Professional Psychology: Research and Practice, 40*(5), 532-538. doi:http://dx.doi.org/10.1037/a0015808

Forskrift om bruk av dyr i forsøk (2015). *Kapittel IV. Krav om hvilke dyr som kan brukes i forsøk.* Retrieved from https://lovdata.no/dokument/SF/forskrift/2015-06-18-761.

Frane, A. V. (2015). Are Per-Family Type I Error Rates Relevant in Social and Behavioral Science? *Journal of Modern Applied Statistical Methods, 14*(1), 12-23.

Galizia, C. G., & Rössler, W. (2010). Parallel olfactory systems in insects: anatomy and function. *Annual review of entomology, 55*, 399-420. doi:10.1146/annurev-ento-112408-085442

Galizia, C. G., Sachse, S., & Mustaparta, H. (2000). Calcium responses to pheromones and plant odours in the antennal lobe of the male and female moth *Heliothis virescens*. *Journal of comparative Physiology A, 186*(11), 1049-1063. doi:10.1007/s003590000156

Gao, Q., Yuan, B., & Chess, A. (2000). Convergent projections of *Drosophila* olfactory neurons to specific glomeruli in the antennal lobe. *Nature neuroscience, 3*(8), 780-785. doi:10.1038/77680

Hansson, B. S. (1995). Olfaction in *Lepidoptera*. *Experientia, 51*(11), 1003-1027. doi:10.1007/BF01946910

Harris, K. D., Henze, D. A., Csicsvari, J., Hirase, H., & Buzsáki, G. (2000). Accuracy of tetrode spike separation as determined by simultaneous intracellular and extracellular measurements. *Journal of Neurophysiology, 84*(1), 401-414.

Hartlieb, E., Anderson, P., & Hansson, B. S. (1999). Appetitive learning of odours with different behavioural meaning in moths. *Physiology & behavior, 67*(5), 671-677. doi:http://doi.org/10.1016/S0031-9384(99)00124-9

Heinze, S., Pfuhl, G., & el Jundi, B. (2015). Insect Brain Database. Retrieved from https://www.insectbraindb.org/

Hochner, B., Klein, M., Schacher, S., & Kandel, E. R. (1986). Action-potential duration and the modulation of transmitter release from the sensory neurons of *Aplysia* in presynaptic facilitation and behavioral sensitization. *Proceedings of the National Academy of Sciences, 83*(21), 8410-8414.

Hodgkin, A., & Huxley, A. (1952). The components of membrane conductance in the giant axon of *Loligo*. *The Journal of physiology, 116*(4), 473-496. doi:10.1113/jphysiol.1952.sp004718

Homberg, U., Montague, R., & Hildebrand, J. G. (1988). Anatomy of antenno-cerebral pathways in the brain of the sphinx moth *Manduca sexta*. *Cell and Tissue Research, 254*(2), 255-281. doi:10.1007/BF00225800

Ian, E., Berg, A., Lillevoll, S. C., & Berg, B. G. (2016a). Antennal-lobe tracts in the noctuid moth, *Heliothis virescens*: new anatomical findings. *Cell and Tissue Research, 366*(1), 23-35. doi:10.1007/s00441-016-2448-0

Ian, E., Zhao, X. C., Lande, A., & Berg, B. G. (2016b). Individual Neurons Confined to Distinct Antennal-Lobe Tracts in the *Heliothine* Moth: Morphological Characteristics and Global Projection Patterns. *Frontiers in Neuroanatomy, 10* (101), 1-19. doi:10.3389/fnana.2016.00101

Ioannidis, J. P. (2005). Why most published research findings are false. *PLos med, 2*(8), e124, 0696-0701. doi:https://doi.org/10.1371/journal.pmed.0020124

Ito, K., Shinomiya, K., Ito, M., Armstrong, J. D., Boyan, G., Hartenstein, V., . . . Jenett, A. (2014). A systematic nomenclature for the insect brain. *Neuron, 81*(4), 755-765. doi:http://doi.org/10.1016/j.neuron.2013.12.017

Izhikevich, E. M. (2000). Neural excitability, spiking and bursting. *International Journal of Bifurcation and Chaos, 10*(06), 1171-1266. doi:http://dx.doi.org/10.1142/S0218127400000840

Kanzaki, R., Arbas, E. A., Strausfeld, N. J., & Hildebrand, J. G. (1989). Physiology and morphology of projection neurons in the antennal lobe of the male moth *Manduca sexta*. *Journal of comparative Physiology A, 165*(4), 427-453. doi:10.1007/BF00611233

Kehat, M., & Dunkelblum, E. (1990). Behavioral responses of male *Heliothis armigera* (*Lepidoptera*: *Noctuidae*) moths in a flight tunnel to combinations of components identified from female sex pheromone glands. *Journal of insect behavior, 3*(1), 75-83. doi:10.1007/BF01049196

Koester, J., & Siegelbaum, S. A. (2013b). Membrane potential and the passive electrical properties of the neuron. In E. R. Kandel, J. H. Schwartz, T. M. Jessel, S. A. Siegelbaum, & A. J. Hudspeth (Eds.), *Principles of Neural Science* (5th ed., pp. 126-147). USA: The McGraw-Hill Companies, Inc.

Koester, J., & Siegelbaum, S. A. (2013a). Propagated Signaling: The Action Potential. In E. R. Kandel, J. H. Schwartz, T. M. Jessel, S. A. Siegelbaum, & A. J. Hudspeth (Eds.), *Principles of Neural Science* (5th ed., pp. 148-171). USA: The McGraw-Hill Companies, Inc.

Lei, H., Christensen, T. A., & Hildebrand, J. G. (2002). Local inhibition modulates odor-evoked synchronization of glomerulus-specific output neurons. *Nature neuroscience, 5*(6), 557-565. doi:10.1038/nn0602-859

Lei, H., Christensen, T. A., & Hildebrand, J. G. (2004). Spatial and temporal organization of ensemble representations for different odor classes in the moth antennal lobe. *Journal of Neuroscience, 24*(49), 11108-11119. doi:https://doi.org/10.1523/JNEUROSCI.3677-04.2004

Lei, H., Reisenman, C. E., Wilson, C. H., Gabbur, P., & Hildebrand, J. G. (2011). Spiking patterns and their functional implications in the antennal lobe of the tobacco hornworm *Manduca sexta*. *PLoS One, 6*(8), e23382, 1-11. doi:https://doi.org/10.1371/journal.pone.0023382

Lisman, J. E. (1997). Bursts as a unit of neural information: making unreliable synapses reliable. *Trends in neurosciences, 20*(1), 38-43. doi:http://doi.org/10.1016/S0166-2236(96)10070-9

Løfaldli, B. B., Kvello, P., Kirkerud, N., & Mustaparta, H. (2012). Activity in neurons of a putative protocerebral circuit representing information about a 10 component plant odor blend in *Heliothis virescens*. *Frontiers in systems neuroscience, 6*, 1-19. doi:https://doi.org/10.3389/fnsys.2012.00064

Masse, N. Y., Turner, G. C., & Jefferis, G. S. (2009). Olfactory information processing in *Drosophila*. *Current Biology, 19*(16), R700-R713. doi:http://doi.org/10.1016/j.cub.2009.06.026

Matsumoto, S., & Hildebrand, J. (1981). Olfactory mechanisms in the moth *Manduca sexta*: response characteristics and morphology of central neurons in the antennal lobes. *Proceedings of the Royal Society of London B: Biological Sciences, 213*(1192), 249-277. doi:10.1098/rspb.1981.0066

Meyer, A., Galizia, C. G., & Nawrot, M. P. (2013). Local interneurons and projection neurons in the antennal lobe from a spiking point of view. *Journal of Neurophysiology, 110*(10), 2465-2474. doi:10.1152/jn.00260.2013

Mohri, M., Rostamizadeh, A., & Talwalkar, A. (2012). *Foundations of machine learning* (pp. 1-9). USA: MIT press.

Moore, G. P., Perkel, D., & Segundo, J. (1966). Statistical analysis and functional interpretation of neuronal spike data. *Annual review of physiology, 28*(1), 493-522. doi:10.1146/annurev.ph.28.030166.002425

Mustaparta, H. (2002). Encoding of plant odour information in insects: peripheral and central mechanisms. *Entomologia Experimentalis et Applicata, 104*(1), 1-13.

Nawrot, M. P. (2010). Analysis and interpretation of interval and count variability in neural spike trains. In S. Grün & S. Rotter (Eds.), *Analysis of parallel spike trains* (pp. 37-58). USA: Springer.

Nawrot, M. P., Boucsein, C., Molina, V. R., Riehle, A., Aertsen, A., & Rotter, S. (2008). Measurement of variability dynamics in cortical spike trains. *Journal of neuroscience methods, 169*(2), 374-390. doi:http://doi.org/10.1016/j.jneumeth.2007.10.013

P-97 Flaming-Brown™ Micropipette Puller Operation Manual. (2016). Retrieved from https://www.sutter.com/manuals/P-97-INT_OpMan.pdf

Perkel, D. H., Gerstein, G. L., & Moore, G. P. (1967). Neuronal spike trains and stochastic point processes: I. The single spike train. *Biophysical journal, 7*(4), 391-418. doi:https://doi.org/10.1016/S0006-3495(67)86596-2

Pfuhl, G., Zhao, X.-C., Ian, E., Surlykke, A., & Berg, B. G. (2014). Sound-sensitive neurons innervate the ventro-lateral protocerebrum of the *Heliothine* moth brain. *Cell and Tissue Research, 355*(2), 289-302. doi:10.1007/s00441-013-1749-9

Reisenman, C. E., Dacks, A. M., & Hildebrand, J. G. (2011). Local interneuron diversity in the primary olfactory center of the moth *Manduca sexta*. *Journal of comparative Physiology A, 197*(6), 653-665. doi:10.1007/s00359-011-0625-x

Rø, H., Müller, D., & Mustaparta, H. (2007). Anatomical organization of antennal lobe projection neurons in the moth *Heliothis virescens*. *Journal of Comparative Neurology, 500*(4), 658-675. doi:10.1002/cne.21194

Sanes, J. R., & Hildebrand, J. G. (1976). Acetylcholine and its metabolic enzymes in developing antennae of the moth, *Manduca sexta*. *Developmental biology, 52*(1), 105-120. doi:https://doi.org/10.1016/0012-1606(76)90011-7

Seki, Y., & Kanzaki, R. (2008). Comprehensive morphological identification and GABA immunocytochemistry of antennal lobe local interneurons in *Bombyx mori*. *Journal of Comparative Neurology, 506*(1), 93-107. doi:10.1002/cne.21528

Seki, Y., Rybak, J., Wicher, D., Sachse, S., & Hansson, B. S. (2010). Physiological and morphological characterization of local interneurons in the *Drosophila* antennal lobe. *Journal of Neurophysiology, 104*(2), 1007-1019. doi:10.1152/jn.00249.2010

Shaffer, J. P. (1995). Multiple hypothesis testing. *Annual review of psychology, 46*(1), 561-584. doi:http://dx.doi.org/10.1146/annurev.ps.46.020195.003021

Shang, Y., Claridge-Chang, A., Sjulson, L., Pypaert, M., & Miesenböck, G. (2007). Excitatory local circuits and their implications for olfactory processing in the fly antennal lobe. *Cell, 128*(3), 601-612. doi:http://doi.org/10.1016/j.cell.2006.12.034

Siegelbaum, S. A., Kandel, E. R., & Yuste, R. (2013). Synaptic integration in the central nervous system. In E. R. Kandel, J. H. Schwartz, T. M. Jessel, S. A. Siegelbaum, & A. J. Hudspeth (Eds.), *Principles of Neural Science* (5th ed., pp. 210-235). USA: The McGraw-Hill Companies, Inc.

Silbering, A. F., & Galizia, C. G. (2007). Processing of odor mixtures in the *Drosophila* antennal lobe reveals both global inhibition and glomerulus-specific interactions. *Journal of Neuroscience, 27*(44), 11966-11977. doi:https://doi.org/10.1523/JNEUROSCI.3099-07.2007

Silbering, A. F., Okada, R., Ito, K., & Galizia, C. G. (2008). Olfactory information processing in the *Drosophila* antennal lobe: anything goes? *Journal of Neuroscience, 28*(49), 13075-13087. doi:https://doi.org/10.1523/JNEUROSCI.2973-08.2008

Stange, G., & Wong, C. (1993). Moth response to climate. *Nature, 365*, 699. doi:10.1038/365699a0

Stopfer, M., Bhagavan, S., Smith, B. H., & Laurent, G. (1997). Impaired odour discrimination on desynchronization of odour-encoding neural assemblies. *Nature, 390*(6655), 70-74. doi:10.1038/36335

Tabuchi, M., Dong, L., Inoue, S., Namiki, S., Sakurai, T., Nakatani, K., & Kanzaki, R. (2015). Two types of local interneurons are distinguished by morphology, intrinsic membrane properties, and functional connectivity in the moth antennal lobe. *Journal of Neurophysiology, 114*(5), 3002-3013. doi:10.1152/jn.00050.2015

Tanaka, N. K., Endo, K., & Ito, K. (2012). Organization of antennal lobe-associated neurons in adult *Drosophila* melanogaster brain. *Journal of Comparative Neurology, 520*(18), 4067-4130. doi:10.1002/cne.23142

van Vreeswijk, C. (2010). Stochastic models of spike trains. In S. Grün & S. Rotter (Eds.), *Analysis of parallel spike trains* (pp. 3-20). USA: Springer.

Watanabe, H., Ai, H., & Yokohari, F. (2012). Spatio-temporal activity patterns of odor-induced synchronized potentials revealed by voltage-sensitive dye imaging and intracellular recording in the antennal lobe of the cockroach. *Frontiers in systems neuroscience, 6*, 55, 1-18. doi:https://doi.org/10.3389/fnsys.2012.00055

Wilson, R. I., & Laurent, G. (2005). Role of GABAergic inhibition in shaping odor-evoked spatiotemporal patterns in the *Drosophila* antennal lobe. *Journal of Neuroscience, 25*(40), 9069-9079. doi:https://doi.org/10.1523/JNEUROSCI.2070-05.2005

Wu, H., Xu, M., Hou, C., Huang, L.-Q., Dong, J.-F., & Wang, C.-Z. (2015). Specific olfactory neurons and glomeruli are associated to differences in behavioral responses

to pheromone components between two *Helicoverpa* species. *Frontiers in behavioral neuroscience, 9*, 206, 1-18. doi:https://doi.org/10.3389/fnbeh.2015.00206

Yasuyama, K., Meinertzhagen, I. A., & Schürmann, F. W. (2002). Synaptic organization of the mushroom body calyx in *Drosophila melanogaster*. *Journal of Comparative Neurology, 445*(3), 211-226. doi:10.1002/cne.10155

Zhang, T. T., Mei, X. D., Feng, J. N., Berg, B. G., Zhang, Y. J., & Guo, Y. Y. (2012). Characterization of three pheromone-binding proteins (PBPs) of *Helicoverpa armigera* (Hübner) and their binding properties. *Journal of insect physiology, 58*(7), 941-948. doi:http://doi.org/10.1016/j.jinsphys.2012.04.010

Zhao, X. C., Chen, Q. Y., Guo, P., Xie, G. Y., Tang, Q. B., Guo, X. G., & Berg, B. G. (2016). Glomerular identification in the antennal lobe of the male moth *Helicoverpa armigera*. *Journal of Comparative Neurology, 524*(15), 2993-3013. doi:10.1002/cne.24003

Zhao, X. C., Kvello, P., Løfaldli, B. B., Lillevoll, S. C., Mustaparta, H., & Berg, B. G. (2014). Representation of pheromones, interspecific signals, and plant odors in higher olfactory centers; mapping physiologically identified antennal-lobe projection neurons in the male *Heliothine* moth. *Frontiers in systems neuroscience, 8*, 186, 1-14. doi:https://doi.org/10.3389/fnsys.2014.00186

Zhao, X. C., Pfuhl, G., Surlykke, A., Tro, J., & Berg, B. G. (2013). A multisensory centrifugal neuron in the olfactory pathway of *Heliothine* moths. *Journal of Comparative Neurology, 521*(1), 152-168.

Zhemchuzhnikov, M. K., Kutcherov, D. A., Kymre, J. H., & Knyazev, A. N. (2017). Louder Songs can Enhance Attractiveness of Old Male Crickets (Gryllus Bimaculatus). *Journal of insect behavior, 30*(2), 211-219. doi:10.1007/s10905-017-9611-7

Appendix A

Morphological overview and figures of selected additional stains

Appendix Table A1

Morphological details of additional stained preparations.

ID	Tract	Cell body	Dendritic arborizations	Terminal projections	Figure	Notes
24/11 m1	ml-, lALT	LCC	MG	LH, AVLP, INP		2 PNs
26/12 m4	AOT	PLP	Lobula	Contralateral VMNP	A1 C	Optical
29/12 m3		LAL	SPS	INP, SNP		
6/1 m3		AD CB	UG	SNP	C1 E	CN
9/1 m1	m-, lALT	ACC & LCC	UG & MG	Ca, LH		2 PNs
18/1 m4 a	mALT	ACC	MG	Ca, LH, AVLP		
18/1 m4 b		AMMC	NC			DN
Mass stains						
30/11 m1	m-, ml-, lALT			Ca, LH, AVLP, CL. P	A1 A	
30/11 m3	m-, ml-, tALT	LCC		Ca, LH, SNP	A1 B	WS
1/12 m2	m-, ml-, l-, tALT			Ca, LH, AVLP		
5/1 m1	m-, ml-, lALT			Ca, LH		
18/1 m1	m-, ml-, lALT, AN	LCC		Ca, VMNP, LH	A1 D	OSNs

Abbreviations: ACC – anterior cell body cluster; AD CB – antero-dorsally to central body; AMMC – antennal mechanosensory and motor center; AN – antennal nerve; AOT – anterior optic tubercle; AVLP – anterior ventromedial protocerebrum; Ca – calyces of the mushroom bodies; CL. P – contralateral projection; CN – centrifugal neuron; DN – descending neuron; INP – inferior neuropil; LAL – lateral accessory lobe; lALT – latera antennal lobe tract; LCC – lateral cell body cluster; LH – lateral horn; mALT – medial antennal lobe tract; MG – multiglomerular; mlALT – mediolateral antennal lobe tract; NC – not conclusive; OSN – olfactory sensory neuron; PLP – posterior lateral protocerebrum; PN – projection neuron; SNP – superior neuropil; SPS – superior posterior slope; tALT – transverse antennal lobe tract; UG – uniglomerular; VMNP – ventro-medial neuropil; WS – weakly stained.

Regarding ID: 6/1 m3

A centrifugal neuron (CN; see appendix Figure C1 E) with neurites extending into the AL was labelled, it may have been an incomplete stain of the CN presented in Zhao, Pfuhl, Surlykke, Tro & Berg (2013). The soma was located in a small cell body cluster antero-dorsally to the central body. One postero-medial glomerulus was innervated, and two other neurites extended dorso-medially into the protocerebrum. Along with this neuron, a mALT PN was weakly stained, leaving the electrophysiological recording unusable, as it could have originated from either neuron.

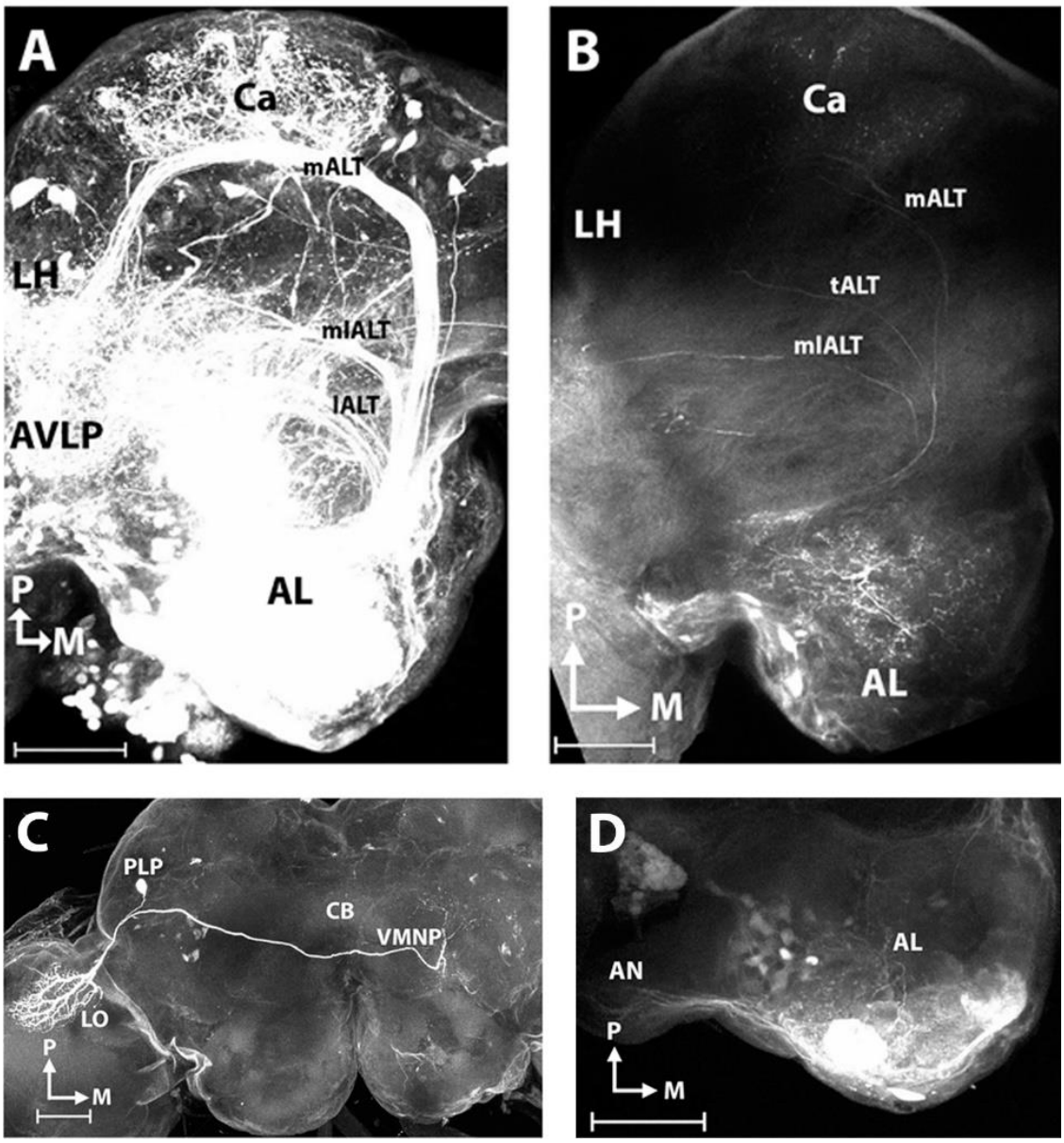

Figure A1. Additional stains, seen from dorsal view. **A)** A massive leakage of dye in the antennal lobe (AL) led to an unintentional mass staining. Displayed are the medial, mediolateral, and lateral antennal lobe tracts (mALT, mlALT and lALT, respectively). **B)** Many lateral cell body cluster neurons were stained, shown are the mALT, mlALT as well as the transverse ALT (tALT). From the tALT, a faint sub-branch running to the calyces can be seen. **C)** A labelled visual neuron, its cell body was found in the posterior lateral protocerebrum (PLP), while dendrites had dense arborizations in the ipsilateral lobula (LO). The axon ran in the anterior optic tubercle (AOT), stretching through the ipsilateral protocerebrum, then anterior to the central body (CB), before innervating the contralateral ventro-medial neuropil (VMNP). **D)** A mass staining of lateral parts of the antennal lobe (AL) led to olfactory sensory neurons (OSNs) in the antennal nerve (AN) being labelled. While several glomeruli seemed to be innervated by the OSNs, two anteriorly positioned glomeruli were particularly heavily innervated. Not presented here, were the medial, mediolateral and lateral antennal lobe tracts, which were also labelled. AL – antennal lobe; AVLP – anterior ventro-lateral protocerebrum; Ca – calyces of the mushroom body; LH – lateral horn. Scale bars: 100 μm.

Appendix B

Morphological overview of neurons provided by Xi Chu

Appendix Table B1

Overview of neurons gathered by Xi Chu, which were used in statistical analyses.

ID	Neuron type	Cell body	Dendritic arborizations	Tract	Notes	Figure
170916	PN	LCC	UG	lALT		
151216	PN	LCC	UG	lALT		
291216M2	PN	NC	UG	lALT		
230117M1_3 MR	PN	LCC	UG	lALT	3 PNs*	
141016M2	PN	MCC	MG	mALT		
191016	PN	LCC	UG	mALT		
211116M3	PN	NC	NC	mALT		
231116M2ME	PN	MCC	UG	mALT		
091216M2	PN	NC	UG	mALT		
271216M3	PN	NC	UG	mALT	2 PNs*	
131216M1	PN	NC	MG	mALT		
120117M2	PN	MCC	UG	mALT		
170117M1	PN	LCC	NC	mALT	2 PNs*	
230117M1_3 AF4	PN	MCC	UG	mALT		
160117M1	PN	LCC	MG	mlALT		
091116M1	PN	LCC	NC	NC		
161116	LN	LCC	MG			
171116M1	LN	LCC	MG			
171116M2	LN	LCC	NC			
231116M2MR	LN	LCC	NC			
020317M3	LN	LCC	MG			
210217M2	LN	LCC	MG		3 LNs*	Fig 9
230217AF488	LN	LCC	MG			

Note: * = Statistically analyzed as one neuron.
Abbreviations: lALT – lateral antennal lobe tract; LCC – lateral cell body cluster; LN – local interneuron; mALT – medial antennal lobe tract; MCC – medial cell body cluster; MG – multiglomerular; mlALT – mediolateral antennal lobe tract; NC – not conclusive; PN – projection neuron; UG – uniglomerular.

Appendix C

Medial tract neurons and a centrifugal neuron

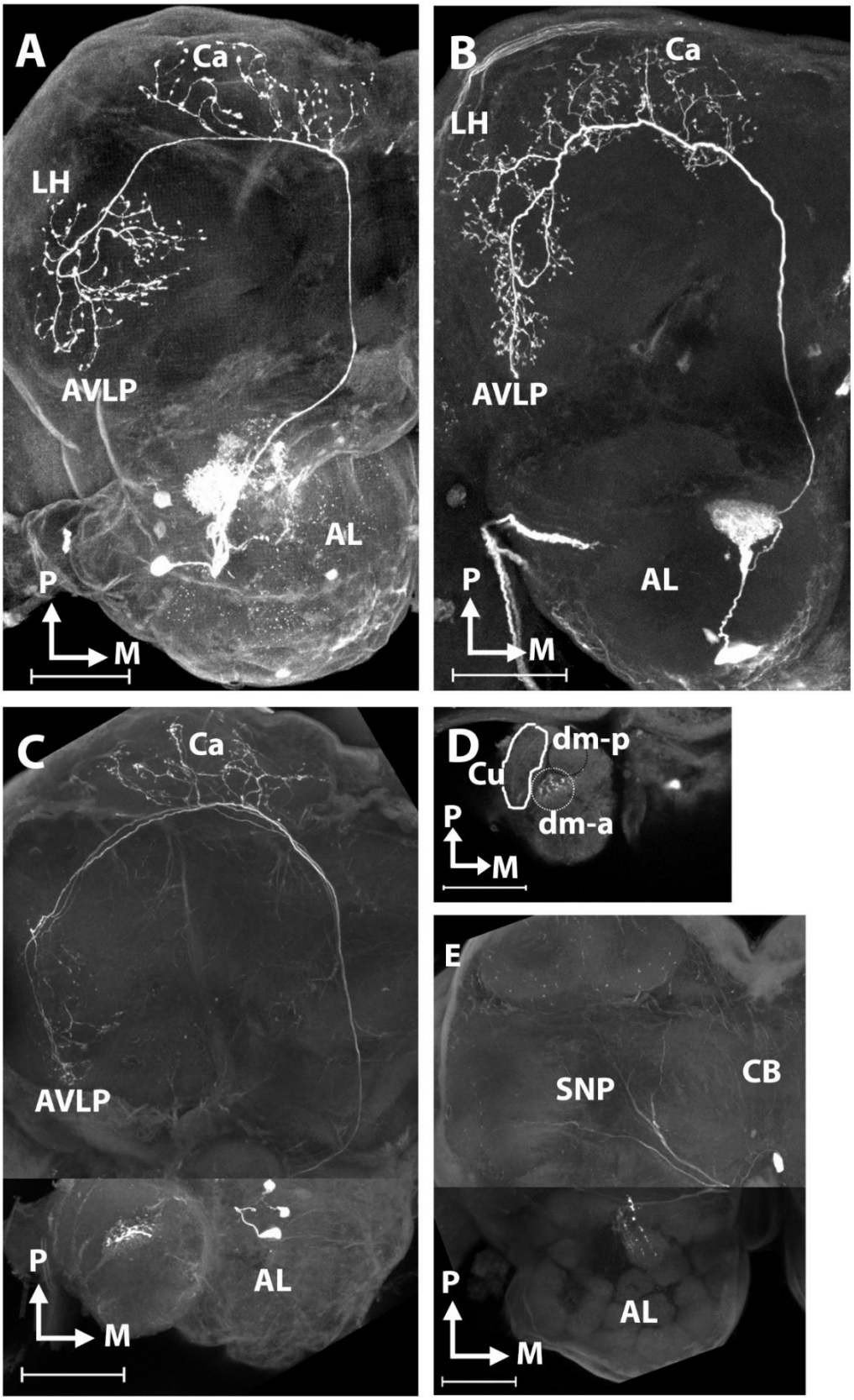

Figure C1. Confocal images of projection neurons (PNs) and an unclassified neuron, seen from dorsal view. **A)** An image of a uniglomerular medial tract (mALT) PN (ID: 26/12 m5), with the cell body located in the lateral cell body cluster (LCC) of the antennal lobe (AL). Axonal innervations were found in the calyces (Ca), the lateral horn (LH) the anterior ventro-lateral neuropil (AVLP) and the inferior neuropil (INP). **B)** Another mALT PN (ID: 9/1 m3), this neuron had a large cell body located in the sparsely populated anterior cell body cluster (ACC). The neuron projected to the calyces, LH and AVLP, where the density of axon terminals was quite high. **C)** Three homogeneous mALT PNs (ID: 28/12 m3), with somata in the LCC and dendrites in the macroglomerular complex (MGC). Projection terminals were seen in the calyces, the LH and the AVLP. **D)** A closer view of the PNs in **C**. Dendrites are assumed to be seen in the anterior dorso-medial unit (dm-a; white dotted circle), while the posterior dorso-medial unit (dm-p; black dotted circle) and the cumulus (Cu; delimited in solid white) are also marked. As the lateral AL was slightly distorted, which MGC sub-unit was innervated cannot be confirmed beyond doubt. **E)** Two merged images display a centrifugal neuron (ID: 6/1 m3), with its soma located antero-dorsally to the central body (CB). One neurite arborizes in a postero-medial glomerulus, while two other neurites extend into the superior neuropil (SNP). Scale bars: 100 µm.

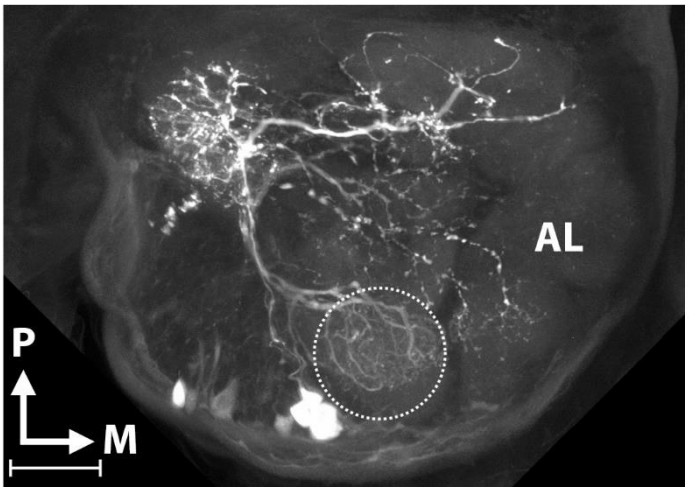

Figure C2: In this preparation, several local interneurons (LNs) were stained, displayed here is a confocal image of the LN which emitted the strongest fluorescence. The LN had its cell body in the lateral cell body cluster (LCC). As all other antennal lobe (AL) LNs, the neurons were confined to the AL. The glomerular innervation pattern was asymmetric, and most glomeruli were sparsely innervated. Two glomeruli, however, were particularly strongly innervated, i.e. a posteriorly situated glomerulus, as well as the labial-palp pit organ glomerulus (LPOG; white dotted circle). Scale bar: 50 µm.

Appendix D

Overview and examples of responses to odor stimulation

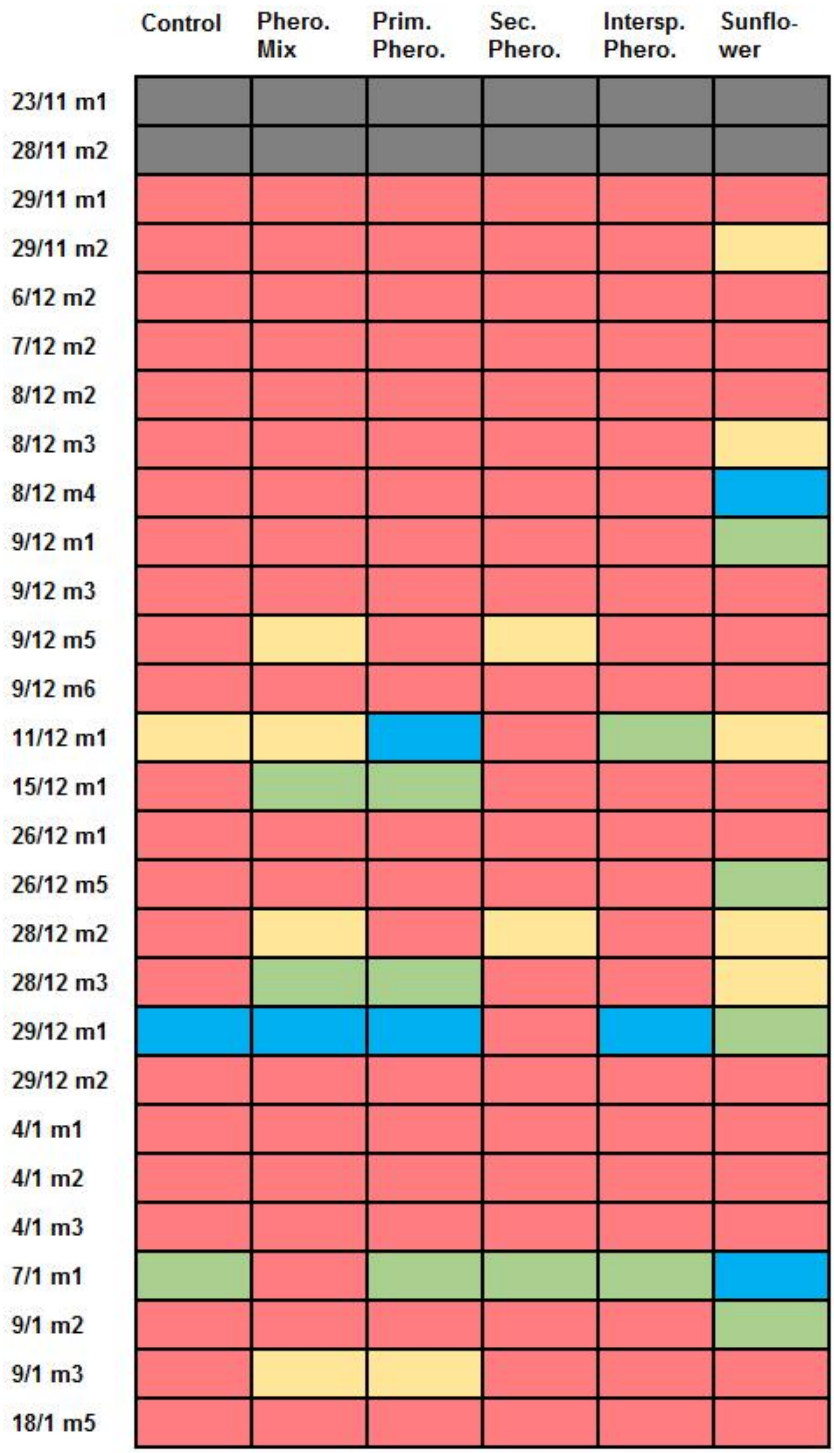

Figure D1. Overview of responses, based on visual inspection. Green – excitatory response; yellow – inhibitory response; blue – complex response; red – no response; grey – excessive noise impedes response detection.

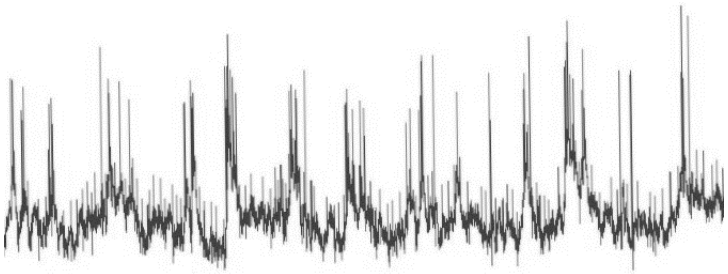

Figure D2. An example of multiple waveforms, which were strongly dissimilar and indicative of contact with more than one neuron. This neuron (ID: 23/11 m1) was excluded from statistical and response analyses.

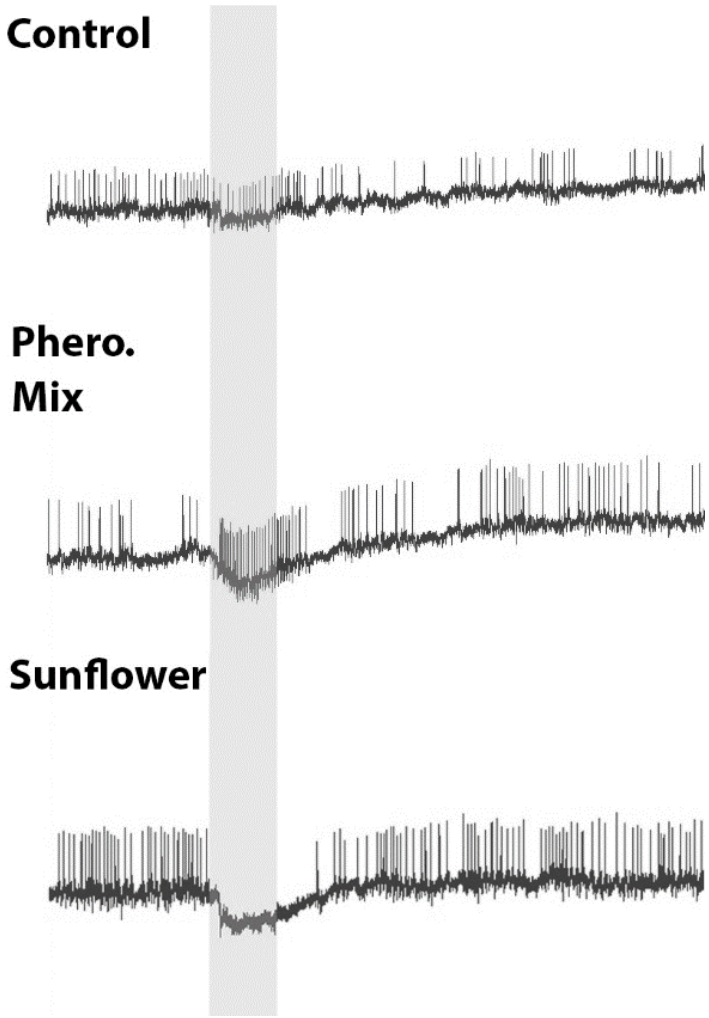

Appendix Figure D3. Examples of responses to odor stimulation (ID: 28/12 m3). The entire 4000 ms stimulation windows are displayed, with 1000 ms pre-stimulation period showing spontaneous activity, 400 ms stimulation (grey bars), as well as 2600 ms post-stimulation periods. When stimulated with control, there was no noteworthy change in firing rate, while the pheromone mixture elicited excitatory responses, here outlasting the stimulation window by ~180 ms. For stimulation with sunflower, there were clear inhibitory responses.

Appendix E

Parameter values for all neurons included in statistical analyses, sorted by ID

Appendix Table E1

Overview of parameter values for individual neurons included in statistical analyses

ID	Spontaneous firing rate	Fano Factor	ISI Mean	ISI cV	FWHM	Spike duration
29/11 m1	28,092	1,406	8,650	0,555	0,983	2,419
6/12 m2	15,500	3,530	6,800	0,871	0,323	0,628
7/12 m2	6,778	3,165	1,700	0,691	0,584	1,164
8/12 m2	26,917	0,707	20,950	1,235	0,870	1,751
8/12 m3	11,722	0,225	5,700	0,595	0,394	0,710
8/12 m4	20,736	0,895	20,350	0,960	0,360	0,658
9/12 m1	11,389	0,989	10,150	0,847	0,458	0,839
9/12 m3	3,820	4,933	3,650	0,886	1,008	1,820
9/12 m5	15,139	0,937	9,600	0,951	0,502	0,918
9/12 m6	2,472	0,123	0,900	1,075	0,327	0,623
11/12 m1	11,333	3,155	9,600	0,865	0,355	0,791
15/12 m1	15,000	0,836	12,000	1,097	0,422	0,742
26/12 m1	8,278	1,445	66,550	0,680	0,550	0,970
26/12 m5	12,972	3,221	7,250	0,848	0,499	0,905
28/12 m2	12,333	1,524	8,050	0,364	0,421	0,768
28/12 m3	17,667	0,936	12,300	1,033	1,101	2,029
29/12 m1	9,056	1,013	5,400	0,686	0,587	1,088
29/12 m2	11,500	4,111	11,150	0,906	0,639	1,155
4/1 m1	47,944	0,701	46,350	1,800	1,430	2,500
4/1 m3	10,667	0,513	6,450	1,436	0,444	0,819
7/1 m1	16,167	0,854	14,600	0,883	0,450	0,764
9/1 m2	21,389	1,241	21,200	0,952	0,542	1,038
9/1 m3	56,611	2,180	49,100	1,964	1,073	2,063
170916	32,556	8,188	18,750	1,400	1,039	1,894
141016M2	7,812	0,232	20,950	1,069	1,523	2,671
191016	22,313	0,478	26,100	1,199	1,371	2,740
091116M1	8,639	1,494	5,350	0,922	0,334	0,803
161116M1	13,344	0,560	10,750	1,090	0,464	0,853
171116M1	7,625	8,817	1,700	1,064	0,425	0,828
171116M2	13,890	0,823	8,400	1,090	0,397	0,732
211116M3	20,333	1,515	15,500	0,595	0,390	0,774
231116M2MR	49,611	0,314	29,900	1,518	0,385	0,652

231116M2ME	30,139	0,273	21,900	1,062	0,687	1,256
091216M2	19,120	0,247	16,550	0,645	0,457	0,813
131216M1	26,717	0,248	23,800	1,308	0,942	1,899
151216	32,083	0,971	31,550	1,255	0,418	0,712
271216M3	16,458	0,034	28,900	1,061	0,694	1,450
291216M2	20,961	0,303	14,400	0,809	0,477	0,827
120117M2	25,472	0,435	24,300	1,220	0,398	0,738
160117M1	23,931	0,453	28,700	0,840	0,475	0,843
170117M1	20,338	2,965	27,200	0,661	0,440	0,823
230117M1_3 MR	22,606	0,004	37,400	0,809	0,375	0,696
230117M1_3 AF4	22,606	0,004	16,350	0,860	0,673	1,169
020317M3	29,906	0,482	45,450	1,009	0,941	2,111
210217M2	13,861	0,063	15,100	0,731	1,392	2,584
230217AF488	23,031	0,152	26,900	0,928	2,859	4,730

Abbreviations: cV – coefficient of variance; FWHM – full-width at half maximum; ISI – interspike interval.